

**A mosaic of phytoplankton responses across Patagonia, the southeast Pacific and southwest Atlantic Oceans to ash deposition and trace metal release from the Calbuco volcanic eruption in 2015**

Maximiliano J. Vergara-Jara<sup>1,2</sup>, Mark J. Hopwood<sup>3\*</sup>, Thomas J. Browning<sup>3</sup>, Insa Rapp<sup>4</sup>, Rodrigo Torres<sup>2,5</sup>, Brian Reid<sup>5</sup>, Eric P. Achterberg<sup>3</sup>, José Luis Iriarte<sup>2,6</sup>.

<sup>1</sup>Programa de Doctorado en Ciencias de la Acuicultura, Universidad Austral de Chile, Puerto Montt, Chile.

<sup>2</sup>Instituto de Acuicultura & Centro de Investigación Dinámica de Ecosistemas Marinos de Altas Latitudes - IDEAL, Universidad Austral de Chile, Puerto Montt, Chile.

<sup>3</sup>GEOMAR, Helmholtz Centre for Ocean Research, 24148 Kiel, Germany.

<sup>4</sup>Department of Biology, Dalhousie University, Halifax, Nova Scotia, Canada

<sup>5</sup>Centro de Investigación en Ecosistemas de la Patagonia (CIEP), Coyhaique, Chile.

<sup>6</sup>COPAS-Sur Austral, Centro de Investigación Oceanográfica en el Pacífico Sur-Oriental (COPAS), Universidad de Concepción, Concepción, Chile.

Key words: volcanic ash, iron, Fe(II), phytoplankton, carbonate chemistry, Reloncaví Fjord

Corresponding author\*: [mhopwood@geomar.de](mailto:mhopwood@geomar.de)

**Formatted:** Font color: Black

**Formatted:** Normal, Border: Top: (No border), Bottom: (No border), Left: (No border), Right: (No border), Between : (No border), Tab stops: 3.25", Centered + 6.5", Right

37

## 38 **Abstract**

39 Following the eruption of the Calbuco volcano in April 2015, an extensive ash plume spread  
40 across northern Patagonia and into the southeast Pacific and southwest Atlantic Oceans. Here  
41 we report on field surveys conducted in the coastal region receiving the highest ash load  
42 following the eruption (Reloncaví Fjord). The fortuitous location of a long-term monitoring  
43 station in Reloncaví Fjord provided data to evaluate inshore phytoplankton bloom dynamics  
44 and carbonate chemistry during April-May 2015. Satellite derived chlorophyll-a  
45 measurements over the ocean regions affected by the ash plume in May 2015 were obtained  
46 to determine the spatial-temporal gradients in offshore phytoplankton response to ash.  
47 Additionally, leaching experiments were performed to quantify the release from ash into  
48 solution of total alkalinity, trace elements (dissolved Fe, Mn, Pb, Co, Cu, Ni and Cd) and  
49 major ions (~~HF~~,  $\text{Cl}^-$ ,  $\text{SO}_4^{2-}$ ,  $\text{NO}_3^-$ ,  $\text{Li}^+$ ,  $\text{Na}^+$ ,  $\text{NH}_4^+$ ,  $\text{K}^+$ ,  $\text{Mg}^{2+}$ ,  $\text{Ca}^{2+}$ ). Within Reloncaví Fjord,  
50 integrated peak diatom abundances during the May 2015 austral bloom were approximately  
51 2-4 times higher than usual (up to  $1.4 \times 10^{11}$  cells  $\text{m}^{-2}$ , integrated to 15 m depth), with the  
52 bloom intensity perhaps moderated due to high ash loadings in the two weeks following the  
53 eruption. Any mechanistic link between ash deposition and the Reloncaví diatom bloom can  
54 however only be speculated on due to the lack of data immediately preceding and following  
55 the eruption. In the offshore southeast Pacific, a short duration phytoplankton bloom  
56 corresponded closely in space and time to the maximum observed ash plume, potentially in  
57 response to Fe-fertilization of a region where phytoplankton growth is typically Fe-limited  
58 at this time of year. Conversely, no clear fertilization on the same time-scale was found in  
59 the area subject to an ash plume over the southwest Atlantic where the availability of fixed

**Formatted:** Font color: Black

**Formatted:** Normal, Border: Top: (No border), Bottom: (No border), Left: (No border), Right: (No border), Between : (No border), Tab stops: 3.25", Centered + 6.5", Right

60 nitrogen is thought to limit phytoplankton growth. This was consistent with no significant  
61 release of fixed nitrogen ( $\text{NO}_x$  or  $\text{NH}_4$ ) from ~~the~~Calbuco ash.

62

63 In addition to release of nanomolar concentrations of dissolved Fe from ash suspended in  
64 seawater, it was observed that low loadings ( $< 5 \text{ mg L}^{-1}$ ) of ash were an unusually prolific  
65 source of Fe(II) into chilled seawater (up to  $1.0 \mu\text{mol Fe g}^{-1}$ ), producing a pulse of Fe(II)  
66 typically released mainly during the first minute after addition to seawater. This release  
67 would not be detected, either as Fe(II) or dissolved Fe, following standard leaching protocols  
68 at room temperature. A pulse of Fe(II) release upon addition of Calbuco ash to seawater made  
69 it an unusually efficient dissolved Fe source ~~with the ~18-38%. The~~ fraction of dissolved Fe  
70 released as Fe(II) from Calbuco ash (~18-38%) was roughly comparable to literature values  
71 for Fe released into seawater from aerosols collected over the Pacific Ocean ~~which have been~~  
72 ~~substantially moderated by photochemical processing following long range atmospheric~~  
73 transport.

**Formatted:** Font color: Black

**Formatted:** Normal, Border: Top: (No border), Bottom: (No border), Left: (No border), Right: (No border), Between : (No border), Tab stops: 3.25", Centered + 6.5", Right

## 1. Introduction

Volcanic ash has long been considered a large, intermittent source of trace metals to the ocean (Frogner et al., 2001; Sarmiento, 1993; Watson, 1997) and its deposition is now deemed a sporadic generally low-macronutrient, high-micronutrient supply mechanism (Ayrís and Delmelle, 2012; Jones and Gislason, 2008; Lin et al., 2011). As volcanic ash can be a regionally significant source of allochthonous inorganic material to affected water bodies, volcanic eruptions have the potential to dramatically change light availability, the carbonate system, properties of sinking particles and ecosystem dynamics (Hoffmann et al., 2012; Newcomb and Flagg, 1983; Stewart et al., 2006). Surveys directly underneath the ash plume from the 2010 eruption of Eyjafjallajökull (Iceland) over the North Atlantic found, among other biogeochemical perturbations, high dissolved Fe (dFe) concentrations of up to 10 nM in affected surface seawater (Achterberg et al., 2013) which could potentially result in enhanced primary production. The greatest potential positive effect of ash deposition on marine productivity would generally be expected in high-nitrate, low-chlorophyll (HNLC) areas of the ocean (Hamme et al., 2010; Mélançon et al., 2014), where low Fe concentrations are a major factor limiting primary production (Martin et al., 1990; Moore et al., 2013). Special interest is therefore placed on the ability of volcanic ash to release dFe, and other bio-essential trace metals such as Mn (Achterberg et al., 2013; Browning et al., 2014; Hoffmann et al., 2012), into seawater. In contrast, apart from inducing light limitation, there are several adverse effects of ash deposition on aquatic organisms. These include metal toxicity (Ermolin et al., 2018), particularly under high dust loading (Hoffmann et al., 2012), and the ingestion of ash particles by filter feeders, phagotrophic organisms or fish (Newcomb and Flagg, 1983; Wolinski et al., 2013). Transient shifts to low pH have also been reported

**Formatted:** Font color: Black

**Formatted:** Normal, Border: Top: (No border), Bottom: (No border), Left: (No border), Right: (No border), Between : (No border), Tab stops: 3.25", Centered + 6.5", Right

in some, but not all, ash leaching experiments and in some ~~fresh-waterbodies~~freshwater  
bodies following intense ash falls, suggesting that significant ash deposition on weakly  
buffered aquatic environments can also impact and perturb their carbonate system (Duggen  
et al., 2010; Jones and Gislason, 2008; Newcomb and Flagg, 1983). The greatest negative  
impact of ash on primary producers would therefore be expected closest to the source where  
the ash loading is highest and in areas where macronutrients or light, rather than trace  
elements, limit primary production.

In contrast to the ~~North Atlantic 2013~~2010 Eyjafjallajökull plume over the North Atlantic,  
the 2015 ash plume over the region from the Calbuco eruption (northern Patagonia, Chile)  
was predominantly deposited ~~largely~~ over an inshore and coastal region (Romero et al., 2016)  
(Fig. 1). This led to visible high ash loadings in affected surface waters in the weeks after the  
eruption (Fig. 2), providing a case study for a concentrated ash deposition event in a coastal  
system; Reloncaví Fjord, which is the northernmost fjord of Patagonia. It receives the direct  
discharge from three major rivers, creating a highly stratified and productive fjord system in  
terms of both phytoplankton biomass and aquaculture production of mussels (González et  
al., 2010; Molinet et al., 2017; Yevenes et al., 2019). Here we combine in situ observations  
from moored arrays which were fortuitously deployed in Reloncaví Fjord (Vergara-Jara et  
al., 2019), with satellite-derived chlorophyll data for offshore regions subject to ash  
deposition, and leaching experiments carried out on ash collected from the fjord region, to  
investigate the inorganic consequences of ash addition to ~~solution~~natural waters. We thereby  
evaluate the potential positive and negative effects of ash from the 2015 Calbuco eruption on

Formatted: Tab stops: 4.06", Left

Formatted: Font color: Black

Formatted: Normal, Border: Top: (No border), Bottom: (No border), Left: (No border), Right: (No border), Between : (No border), Tab stops: 3.25", Centered + 6.5", Right

marine primary production in three geographical regions; Reloncaví Fjord and the areas of the SE Pacific and SW Atlantic Oceans beneath the most intense ash plume.

## 2. Materials and methods

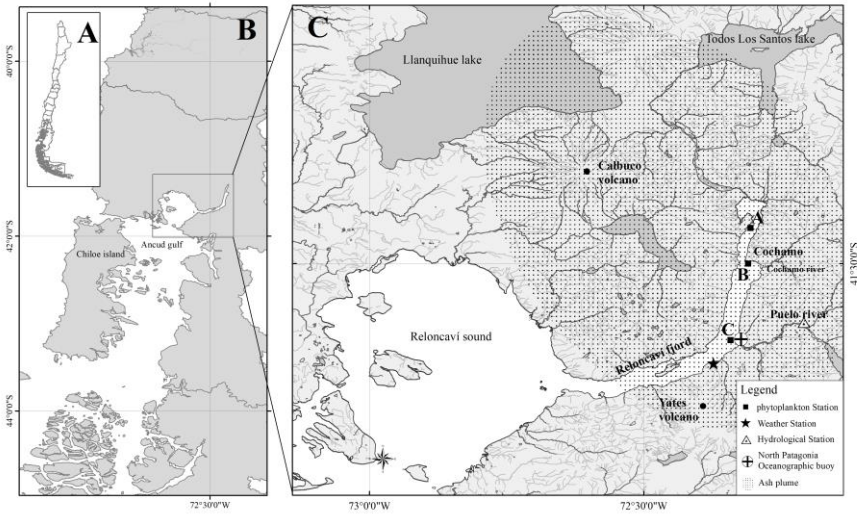
### 2.1. Study area

The Calbuco volcano (Fig. 1) is located in a region with large freshwater reservoirs and a major river (the Petrohué) that flows into in close proximity to Reloncaví Fjord. The predominant bedrock type is andesite (López-Escobar et al., 1995). Reloncaví Fjord is 55 km long and receives freshwater from 3 main rivers, the Puelo, Petrohué, and Cochamó, with mean stream flows of  $650 \text{ m}^3 \text{ s}^{-1}$ ,  $350 \text{ m}^3 \text{ s}^{-1}$  and  $100 \text{ m}^3 \text{ s}^{-1}$ , respectively (León-Muñoz et al., 2013). ~~River discharge strongly influences seasonal patterns of primary production across the region, supplying silicic acid and strongly stratifying the water column (Castillo et al., 2016; González et al., 2010; Torres et al., 2014)~~River discharge strongly influences seasonal patterns of primary production across the region, supplying silicic acid and strongly stratifying the water column (Castillo et al., 2016; González et al., 2010; Torres et al., 2014). Seasonal changes in light availability rather than macronutrient supply are thought to control marine primary production across the Reloncaví region with high marine primary production ( $>1 \text{ g C m}^{-2} \text{ day}^{-1}$ ) throughout austral spring, summer and early autumn (González et al., 2010).

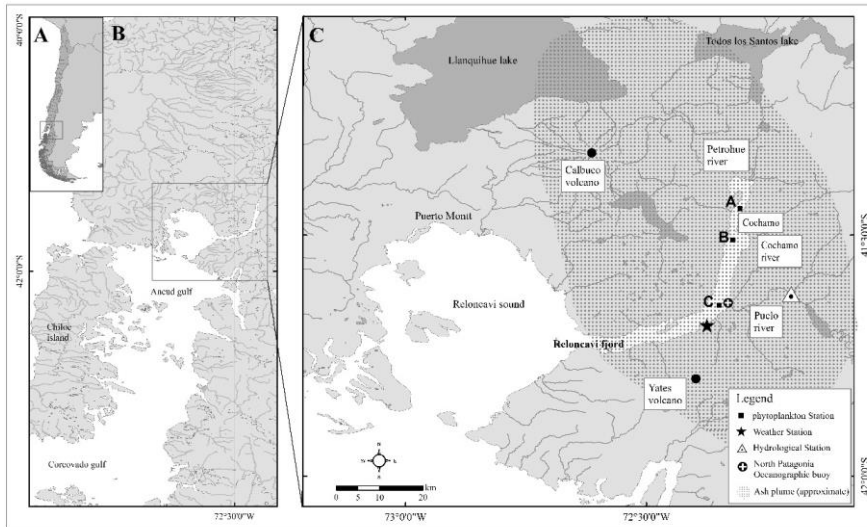
Formatted: None

Formatted: Font color: Black

Formatted: Normal, Border: Top: (No border), Bottom: (No border), Left: (No border), Right: (No border), Between : (No border), Tab stops: 3.25", Centered + 6.5", Right



139



140

7  
7

Formatted: Font color: Black

Formatted: Normal, Border: Top: (No border), Bottom: (No border), Left: (No border), Right: (No border), Between : (No border), Tab stops: 3.25", Centered + 6.5", Right

Figure 1. The Calbuco region showing the location of Reloncaví Fjord, 3 major rivers (Petrohué, Cochamó and Puelo) discharging into the fjord, the 3 stations (black squares; A, B and C) used to assess changes in phytoplankton abundance following the eruption, a hydrological station that monitors Puelo river flow, a weather station and the location of a long-term mooring within the fjord. The approximate extent of the ash plume in the week following the first eruption is illustrated, as estimated in technical reports issued by the Servicio Nacional de Geología y Minería- (Chile).

On 22 April 2015 the Calbuco volcano erupted after 54 years of dormancy. Two major eruption pulses lasted <2 hours on 22 April and 6 hours on 23 April, releasing a total volume of 0.27 km<sup>3</sup> ash which was projected up to 20 km height above sea level (Van Eaton et al., 2016; Romero et al., 2016). Ash layers of several cm thick were deposited mainly to the NE of the volcano in subsequent days (Romero et al., 2016). A smaller eruption occurred on 30 April projecting ash 4-5 km above sea level which was then mainly deposited south of the volcano. Smaller volumes of ash were released semi-continuously for three weeks after the main eruption, leading to intermittent ash deposition events. Fortunately, as part of a long-term deployment, an ocean acidification buoy in the middle of Reloncaví Fjord (Vergara-Jara et al., 2019) and an associated meteorological station close to the volcano (Fig. 1) were well placed to assess the impact of ash fall immediately after the eruption. To ~~complement~~complement data from these facilities, after the regional evacuation order was removed, weekly sampling campaigns were conducted in the fjord commencing one week after the eruption. The Chilean Geological-mining Survey (Servicio Nacional de Geología y Minería, SERNAGEOMIN) produced daily technical reports including the estimated area of

Formatted: None

Formatted: Font color: Black

Formatted: Normal, Border: Top: (No border), Bottom: (No border), Left: (No border), Right: (No border), Between : (No border), Tab stops: 3.25", Centered + 6.5", Right



ash dispersion (<http://sitiohistorico.sernageomin.cl/volcan.php?pagina=4&iId=3>). This information was used to create a reference aerial extent of ash deposition for the week after the eruption (Fig. 1, C) and this approximation represents a full week of coverage for this dynamic feature.

## 2.2. Ash samples – trace metal leaching experiments

~~Ash (500 g) was collected (On 6 May (2015, in Cochamó, Chile), approximately 30 km from the volcano) after the third, and smallest, eruptive pulse of ash from the Calbuco volcano (Fig. 2, A), and with the volcano still emitting material, ash was collected using a plastic tray wrapped with plastic sheeting (40 × 94 cm<sup>2</sup>). The plasticware was left outside for 24 hours until sufficient ash (~500 g) was collected to provide a bulk sample. Ambient weather over the period of ash collection, and the preceding day, was dry (no precipitation). The collected ash was~~ double sealed in low density polyethylene (LDPE) plastic bags and stored in the dark. ~~Ambient weather in the day preceding ash collection was dry.~~ A sub-sample was analyzed for particle size using a Mastersizer 2000 at The University of Chile. ~~Offshore~~

~~Ash may affect in situ phytoplankton dynamics in several ways, for example via moderating the carbonate system, macronutrient availability and/or micronutrient availability. As micronutrient (e.g. Fe and Mn) availability is expected to be the main chemical mechanism via which phytoplankton dynamics in the offshore marine environment could be affected, we primarily focus our investigation on the release of dissolved trace metals from ash in seawater for. Yet to rule out other potential affects, we also conduct complementary leaches to assess the significance of changes to total alkalinity and macronutrient availability (Table 1). For~~

Formatted: None, Adjust space between Latin and Asian text, Adjust space between Asian text and numbers

Formatted: Font color: Black

Formatted: Normal, Border: Top: (No border), Bottom: (No border), Left: (No border), Right: (No border), Between : (No border), Tab stops: 3.25", Centered + 6.5", Right

trace metal leaches, a variety of methods have been used in the literature (Duggen et al., 2010; Witham et al., 2005) depending on the purpose of specific studies. De-ionized water leaches with ash loadings that are high in an offshore environmental context are preferable for intercomparison studies. The trace metals released under such conditions are however difficult to compare quantitatively to metal exchange processes in the ambient marine environment, especially for elements such as Fe where solubility is strongly influenced by pH, salinity and the nature of dissolved organic carbon present (Baker and Croot, 2010). For prior work conducted specifically using volcanic ash in seawater, 3 main methods have been employed: suspension experiments followed by analysis of the leachate, flow-through reactors, and continuous voltammetric determination of dFe concentrations in situ during suspension experiments (Sup. Table 1). The most commonly used ash:solute ratio in prior seawater experiments is 1:400 (g:mL), with leach lengths varying from 15 minutes to 24 hours (Sup. Table 1). Conversely, incubation experiments ~~was collected in the~~ designed to test the response of marine phytoplankton to ash deposition have used lower ash:solute ratios of 1:400 to 1:10<sup>7</sup> which are based on estimates of the ash loading expected to be mixed within the offshore surface mixed layer underneath ash plumes (Browning et al., 2014; Hoffmann et al., 2012). Existing data suggests that ash:solute ratio is not a major factor in determining the release behavior of Fe from ash, however this is acknowledged to be difficult to assess due to other differences between experimental setups used to date (Duggen et al., 2010). Both the age of particles since collection and the organic carbon content of seawater are however known to be critical factors influencing the exchange of Fe, and other trace elements, following any aerosol deposition into seawater (Baker and Croot, 2010; Duggen et al., 2010). Whilst UV-treatment of seawater has been used in some experiments (to remove

**Formatted:** Font color: Black

**Formatted:** Normal, Border: Top: (No border), Bottom: (No border), Left: (No border), Right: (No border), Between : (No border), Tab stops: 3.25", Centered + 6.5", Right

a large part of any natural organic ligands present, Duggen et al., 2007; Jones and Gislason, 2008), and a strong synthetic organic ligand added in others (to impede dissolved Fe precipitation, Duggen et al., 2007; Olgun et al., 2011; Simonella et al., 2015), to improve reproducibility and standardisation, these steps are not well suited specifically for investigating the release of Fe(II) from ash. Herein we therefore adopt ash:solute ratios comparable to the lower end of the range used in leaching experiments and comparable to the range used in incubation experiments. Seawater was used after prolonged storage in the dark (to reduce biological activity to low background levels) and without UV treatment (to maintain an environmentally relevant level of natural organic material in solution). A short leaching time (10 minutes + filtration) was adopted to minimize bottle effects and recognising that most prior work suggests a large fraction of Fe release occurs on short timescales (minutes), followed by more gradual changes on timescales of hours to days (Duggen et al., 2007; Frogner et al., 2001; Jones and Gislason, 2008).

A variety of leaches were conducted in de-ionized water, brackish (fjord) water or offshore South Atlantic seawater (Table 1) with the choice of leaching conditions based on the expected environmental significance in different water masses. Offshore oligotrophic seawater for incubation experiments was collected from an underway transect of the mid-South Atlantic (across 40° S) using a towfish and trace metal clean tubing in a 1 m<sup>3</sup> high density polyethylene tank which had been pre-rinsed with 1 M HCl. This water was stored in the dark for >12 months prior to use in leaching experiments- and was filtered (AcroPak1000 capsule 0.8/0.2 µm filters) when subsampling a batch for use in all leaching experiments. All labware for trace metal leaching experiments was pre-cleaned with Mucosol and 1 M HCl. 125 ml LDPE bottles (Nalgene) for trace metal leach experiments were pre-

**Formatted:** None, Adjust space between Latin and Asian text, Adjust space between Asian text and numbers

**Formatted:** Font color: Black

**Formatted:** Normal, Border: Top: (No border), Bottom: (No border), Left: (No border), Right: (No border), Between : (No border), Tab stops: 3.25", Centered + 6.5", Right

232 cleaned using a 3-stage procedure with three de-ionized water (Milli-Q, Millipore,  
233 conductivity  $18.2 \text{ M}\Omega \text{ cm}^{-1}$ ) rinses after each stage (3 days in Mucosol, 1 week in 1 M HCl,  
234 1 week in 1 M  $\text{HNO}_3$ ).

235 Leach experiments were conducted by adding a pre-weighed mass of ash into 100 ml South  
236 Atlantic Seawater, gently mixing the suspension for 10 minutes, and then syringe filtering  
237 the suspension ( $0.2 \mu\text{m}$ , polyvinylidene fluoride, Millipore). Eight different ash loadings  
238 from  $2\text{--}50 \text{ mg L}^{-1}$  were used, selected to be environmentally relevant and comparable to prior  
239 incubation experiments, with each treatment run in triplicate. Samples for dissolved trace  
240 metals (Fe, Cd, Pb, Ni, Cu, Co and Mn) were acidified within 1 day of collection by the  
241 addition of  $140 \mu\text{L}$  concentrated HCl (UPA grade, ROMIL) and analysed by inductively  
242 coupled plasma mass spectroscopy following preconcentration exactly as per Rapp et al.,  
243 (2017).

244 Leach experiments specifically to measure Fe(II) release were conducted in a similar manner  
245 but in cold seawater with continuous in-line analysis ( $5\text{--}7^\circ\text{C}$  see Sup. Table 2) due to the  
246 rapid oxidation rate of Fe(II) at room temperature ( $\sim 21^\circ\text{C}$ ), which makes accurate  
247 measurement of Fe(II) concentrations challenging (Millero et al., 1987). ~~A~~For these  
248 experiments, a pre-weighed mass of ash was added to 250 ml South Atlantic seawater and  
249 manually shaken for approximately one minute. ~~Ash loadings ranged, using an expanded~~  
250 loading range from  $0.2\text{--}4000 \text{ mg L}^{-1}$ . Fe(II) was measured via flow injection analysis using  
251 luminol chemiluminescence (Jones et al., 2013) without pre-concentration or filtration. The  
252 inflow line feeding the flow injection apparatus was positioned inside the ash suspension  
253 immediately after mixing and measurements begun thereafter at 2 minutes resolution.

Formatted: Font color: Black

Formatted: Normal, Border: Top: (No border), Bottom: (No border), Left: (No border), Right: (No border), Between : (No border), Tab stops: 3.25", Centered + 6.5", Right

Reported mean values ( $\pm$  standard deviation) are determined from the Fe(II) concentrations measured 2-30 minutes after adding ash into solution. Calibrations were run daily using standard additions of 0.2-10 nM Fe(II) to aged South Atlantic seawater at the same temperature with integrated peak area used to construct calibration curves. Following each leaching experiment the apparatus was rinsed with 0.1 M HCl (reagent grade) followed by flushing with de-ionized water to ensure the removal of ash particles. Blank measurements before/after Fe(II) measurements from experiments with different ash loadings verified that there was no discernable interference from ash particles in the Fe(II) flow-through measurements. Fe(II) leaches were conducted 2 weeks, 4 months and 9 months after the eruption. Fe(II) leaches 2 weeks after the eruption were run for 30 minutes. Fe(II) leaches after 4 or 9 months were run for 1 hour to further investigate the temporal development of Fe(II) concentration. The trace metal leach experiments (above) were conducted at the same time as the first Fe(II) incubation experiments (2 weeks after ash collection).

For trace metal leaches, the initial (mean  $\pm$  standard deviation) dissolved trace metal concentrations were deducted from the final concentrations, in order to calculate the net change as a result of ash addition. For Fe(II) measurements, background levels of Fe(II) were below detection ( $<0.1$  nM) and so no deduction was made.

### 2.3 Ash samples – de-ionized and brackish water leaching experiments

Fresh brackish sub-surface water from the Patagonia study region was obtained from the Aysén Fjord, at Ensenada Baja (45°21'S: 72°40'W, salinity 16.3), close to the Coyhaique laboratory (Aysén region, Chile) and free from the influence of ash from the 2015 eruption. The oceanographic conditions in these waters are similar to the adjacent Reloncaví fjord

**Formatted:** None, Adjust space between Latin and Asian text, Adjust space between Asian text and numbers

**Formatted:** Font color: Black

**Formatted:** Normal, Border: Top: (No border), Bottom: (No border), Left: (No border), Right: (No border), Between : (No border), Tab stops: 3.25", Centered + 6.5", Right

~~(Cáceres et al., 2002; González et al., 2011). De-ionized water, along with the Aysén fjord~~  
~~brackish water, were used for leaching experiments following recommendations of Witham~~  
~~et al., (2005)(Cáceres et al., 2002). De-ionized water, along with the Aysén fjord brackish~~  
water, were used for leaching experiments using two size fractions of ash following the  
general recommendations of Duggen et al., (2010) and Witham et al., (2005) to consider the  
effects of different size fractions and leachates. Leaches were conducted in 50 ml LDPE  
bottles filled with either 40 ml brackish or DI-water with 4 replicates of each treatment.  
Bottles were incubated inside a mixer at room temperature after the addition of 0.18 g ash,  
using two ash size fractions (<63 µm and 250-1000 µm) which were separated using sieves  
(ASTM e-11 specification, W.S. Tyler). The ~~size~~mass distribution of the ash as determined  
by sieving was 4.54% >2360 µm; 6.85% <-2360 µm and >1000 µm; 31.12% <1000 µm and  
>250 µm; 24.14% <250 µm and >125 µm; 18.04% <125 µm and >63 µm; 15.31% <63 µm.

~~The dominant size fraction by mass was thereby the 250-1000 µm fraction which was~~  
~~analyzed in addition to the finest fraction (<63 µm) with the greatest surface area to mass~~  
~~ratio.~~ The sampling times were at time zero (defined as just after the addition of the ash and  
a few minutes of mixing), 2 h and 24 h later. Leaching experiments conducted with brackish  
water were analyzed for total alkalinity ( $A_T$ ) via a potentiometric titration using reference  
standards (Haraldsson et al., 1997) ensuring a reproducibility of <-2 µmol/kg. For the de-  
ionized water leaching experiment,  $A_T$  was analyzed by titration of unfiltered 5 ml  
subsamples to a pH 4.5 endpoint (Bromocresol Green/Methyl Red) using a Dosimat  
(Metrohm Inc) and 0.02 N  $H_2SO_4$  titrant. Alkalinity was calculated as  $CaCO_3$  equivalents  
following APHA (American Public Health Association) 2005-Methods 2320 (2320  
Alkalinity, titration method). Additional 5 ml subsamples were filtered, stored at 4°C and

**Formatted:** None, Adjust space between Latin and Asian text, Adjust space between Asian text and numbers

**Formatted:** Font color: Black

**Formatted:** Normal, Border: Top: (No border), Bottom: (No border), Left: (No border), Right: (No border), Between : (No border), Tab stops: 3.25", Centered + 6.5", Right

analyzed within 3 days for major ions ( $\text{F}^-$ ,  $\text{Cl}^-$ ,  $\text{SO}_4^{2-}$ ,  $\text{NO}_3^-$ ,  $\text{Li}^+$ ,  $\text{Na}^+$ ,  $\text{NH}_4^+$ ,  $\text{K}^+$ ,  $\text{Mg}^{2+}$ ,  $\text{Ca}^{2+}$ ) using a Dionex<sup>TM</sup> 5000 Ion Chromatography system with Eluent Generation (APHA). All measurements were then corrected for initial water concentrations prior to ash addition. Saturation indices for species in solution following leaching from <63  $\mu\text{m}$  ash particles were obtained from the MINTEQ 3.1. IAP Ion Activity Product chemical equilibrium model (see Sup. Table 6).

Table 1. Summary of different leaching experiments and samples.

Ash/ particle source	Experiment type <del>objective</del> De-ionized water leaches	Brackish (fjord) water	South Atlantic seawater	N° of replicates
<del>Calbuco Volcano ash, sieved &lt;63 <math>\mu\text{m}</math></del>	<del>Total alkalinity, brackish water</del>			4
Calbuco <del>Volcano</del> ash, sieved <63 $\mu\text{m}$	Total alkalinity, ion and <del>nutrient</del> leaching, DI water <del>macronutrients</del>	Total alkalinity		4
<del>Calbuco Volcano ash, sieved 250-1000 <math>\mu\text{m}</math></del>	<del>Total alkalinity, brackish water</del>			4
Calbuco <del>Volcano</del> ash, sieved 250-1000 $\mu\text{m}$	Total alkalinity, ion and <del>nutrient</del> leaching, DI water <del>macronutrients</del>	Total alkalinity		4
<del>Calbuco Volcanic ash, unsieved</del>	<del>Trace metal leaches, S Atlantic seawater</del>			3

Inserted Cells

Inserted Cells

Formatted: Centered, None, Adjust space between Latin and Asian text, Adjust space between Asian text and numbers, Border: Top: (No border), Bottom: (No border), Left: (No border), Right: (No border), Between : (No border)

Formatted Table

Formatted: Centered, None, Space Before: 12 pt, Adjust space between Latin and Asian text, Adjust space between Asian text and numbers

Formatted: Centered, None, Space Before: 12 pt, Adjust space between Latin and Asian text, Adjust space between Asian text and numbers

Inserted Cells

Inserted Cells

Formatted: Centered, None, Space Before: 12 pt, Adjust space between Latin and Asian text, Adjust space between Asian text and numbers

Formatted: Centered, None, Space Before: 12 pt, Adjust space between Latin and Asian text, Adjust space between Asian text and numbers

Inserted Cells

Inserted Cells

Formatted: Centered, None, Space Before: 12 pt, Adjust space between Latin and Asian text, Adjust space between Asian text and numbers

Formatted: Font color: Black

Formatted: Normal, Border: Top: (No border), Bottom: (No border), Left: (No border), Right: (No border), Between : (No border), Tab stops: 3.25", Centered + 6.5", Right

Calbuco <del>Volcanic</del> ash, unsieved			<u>Trace metals, Fe(II) leaches; chilled S Atlantic seawater</u>	<u>4*3 for trace elements, 1 time series for Fe(II)</u>
----------------------------------------------	--	--	------------------------------------------------------------------------------------------	-----------------------------------------------------------------

**Formatted:** Centered, None, Space Before: 12 pt, Adjust space between Latin and Asian text, Adjust space between Asian text and numbers

**Formatted:** Centered, None, Space Before: 12 pt, Adjust space between Latin and Asian text, Adjust space between Asian text and numbers

**Inserted Cells**

**Inserted Cells**

~~\*1 time series of >10 measurements at 2 minute intervals following ash addition into seawater. DI, de-ionized water.~~

## 2.4 Environmental data – continuous Reloncaví Fjord monitoring

**Formatted:** None, Adjust space between Latin and Asian text, Adjust space between Asian text and numbers

High temporal resolution (hourly) in situ measurements were taken ~~simultaneously~~ in the Reloncaví fjord (Fig. 1 C, North Patagonia Oceanographic Buoy) at ~~the surface and at 3 m depth for  $p\text{CO}_2$ , pH, depth, temperature, conductivity and dissolved  $\text{O}_2$~~  using two SAMI sensors that measured spectrophotometric  $\text{CO}_2$  and pH (DeGrandpre et al., 1995; Seidel et al., 2008) (Sunburst Sensors, LLC), and an SBE 37 MicroCAT CTD-ODO (SeaBird Electronics) for temperature, conductivity, depth and dissolved  $\text{O}_2$ , as per Vergara-Jara et al., (2019). Sensor maintenance and quality control is described by Vergara-Jara et al., (2019). The error in  $p\text{CO}_2$  concentrations is estimated to be at most 5% which arises mainly due to a non-linear sensor response and reduced sensitivity at high  $p\text{CO}_2$  levels >1500 ppm (DeGrandpre et al., 1999). The SAMI-pH instruments used an accuracy test instead of a calibration procedure (Seidel et al., 2008). With the broad pH and salinity range found in the fjord, pH values are subject to a maximum error of  $\pm 0.02$  (Mosley et al., 2004).

A meteorological station (HOBO-U30, Fig. 1) measured air temperature, solar radiation, wind speed and direction, rainfall, and barometric pressure every 5 minutes. Puelo River

**Formatted:** Font color: Black

**Formatted:** Normal, Border: Top: (No border), Bottom: (No border), Left: (No border), Right: (No border), Between : (No border), Tab stops: 3.25", Centered + 6.5", Right



streamflow was obtained from the Carrera Basilio hydrological station (Fig. 1), run by Dirección General de Aguas de Chile (<http://snia.dga.cl/BNAConsultas/reportes>).

## 2.5 Field surveys in Reloncaví Fjord post eruption

During May 2015, weekly field campaigns were undertaken in the Reloncaví Fjord. Phytoplankton samples were collected at 3 depths (1 m, 5 m and 10 m) for taxonomic characterization and abundance determination at 3 stations (A, B and C; Fig. 1) using a 5 L Go-Flo bottle. Samples were analyzed using ~~an~~ Olympus CKX41 inverted phase contrast microscope using a 10 ml sedimentation chamber and the Utermöhl method (Utermöhl, 1958). The phytoplankton community composition was then statistically analyzed in R (RStudio V 1.2.5033) using general linear models in order to find statistically significant differences between dates and group abundances. Additionally, as part of a long-term monitoring program at station C (Fig. ~~1~~), ~~on 6 occasions during March-May 2015;1~~, chlorophyll-a samples were retained from 6 depths (1, 3, 5, 7, 10 and 15 m) ~~on 6 occasions during March-May 2015~~. Chlorophyll-a was determined by fluorometry after filtering 250 ml of sampled water through GFF filters (Whatman) ~~by fluorometry~~ as per ~~Welschmeyer (1994)~~ Welschmeyer (1994). Two additional profiles close to Station C were obtained from Yevenes et al., (2019). Integrated chlorophyll-a ( $\text{mg m}^{-2}$ ) and diatom abundance ( $\text{cells m}^{-2}$ ) were determined to 15 m depth. ~~Chlorophyll-a within Reloncaví Fjord is invariably concentrated in the upper ~10 m (González et al., 2010; Yevenes et al., 2019)~~ Chlorophyll-a within Reloncaví Fjord is invariably concentrated in the upper ~10 m (González et al., 2010; Yevenes et al., 2019) and thus, for comparison to prior ~~data~~ reported data integrated to 10 m, only a small difference is anticipated. For all profiles considered herein ~~(Fig. 4)~~, there is a

**Formatted:** Adjust space between Latin and Asian text, Adjust space between Asian text and numbers

**Formatted:** Font color: Black

**Formatted:** Normal, Border: Top: (No border), Bottom: (No border), Left: (No border), Right: (No border), Between : (No border), Tab stops: 3.25", Centered + 6.5", Right

20% difference between integrating to 10 m or 15 m depth.

## 2.6 Satellite data

Daily, 4 km resolution chlorophyll-a images from the MODIS Aqua sensor (OCI algorithm; Hu et al., 2012) were downloaded from the NASA Ocean Color website (<https://oceancolor.gsfc.nasa.gov>) for the period 4 April 2015–2 May 2015. As a proxy for the spatial extent and loading of the ash plume, the UV aerosol index product from the Ozone Monitoring Instrument (OMI) on the EOS-Aura was downloaded for the same time period. Daily images were composited into 5-day mean averages (Fig. 7). Hu et al., 2012) were downloaded from the NASA Ocean Color website (<https://oceancolor.gsfc.nasa.gov>) for the period 4 April 2015–2 May 2015. As the UV Aerosol Index largely reflects strongly UV-absorbing (dust) aerosols (Torres et al., 2007), this was used as a proxy for the spatial extent and loading of the ash plume. The UV aerosol index product from the Ozone Monitoring Instrument (OMI) on the EOS-Aura was downloaded for the same time period. Daily images were composited into 5-day mean averages.

## 3. Results

### 3.1 In situ observations

The Calbuco ash plume reached up to 20 km height and was dispersed hundreds of kilometers across Patagonia and the Pacific and Atlantic Oceans (Fig. 2) (Van Eaton et al., 2016; Reckziegel et al., 2016; Romero et al., 2016). The ash loading in water bodies near the cone was visually observed to be high, especially near the Petrohué river catchment that drains into the head of the Reloncaví fjord. This ash loading into the fjord was clearly visible on 6 May 2015 when ash samples were collected for leaching experiments (Fig. 2).

Formatted: Font color: Black

Formatted: Normal, Border: Top: (No border), Bottom: (No border), Left: (No border), Right: (No border), Between : (No border), Tab stops: 3.25", Centered + 6.5", Right

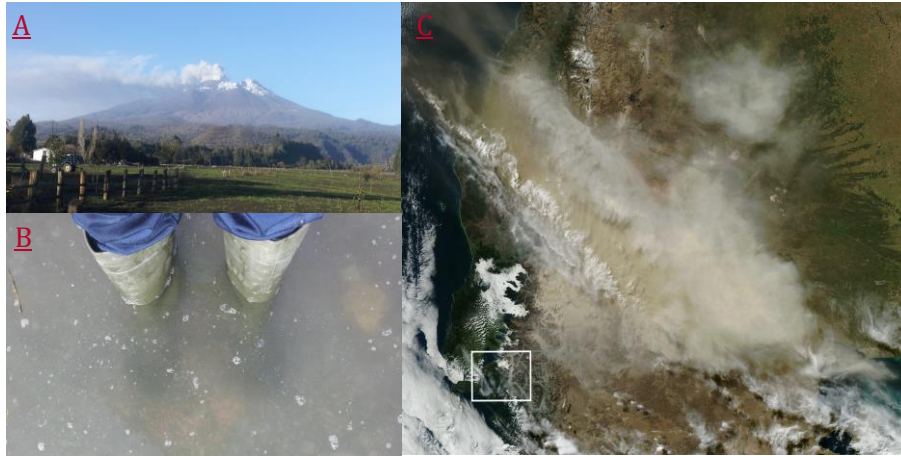
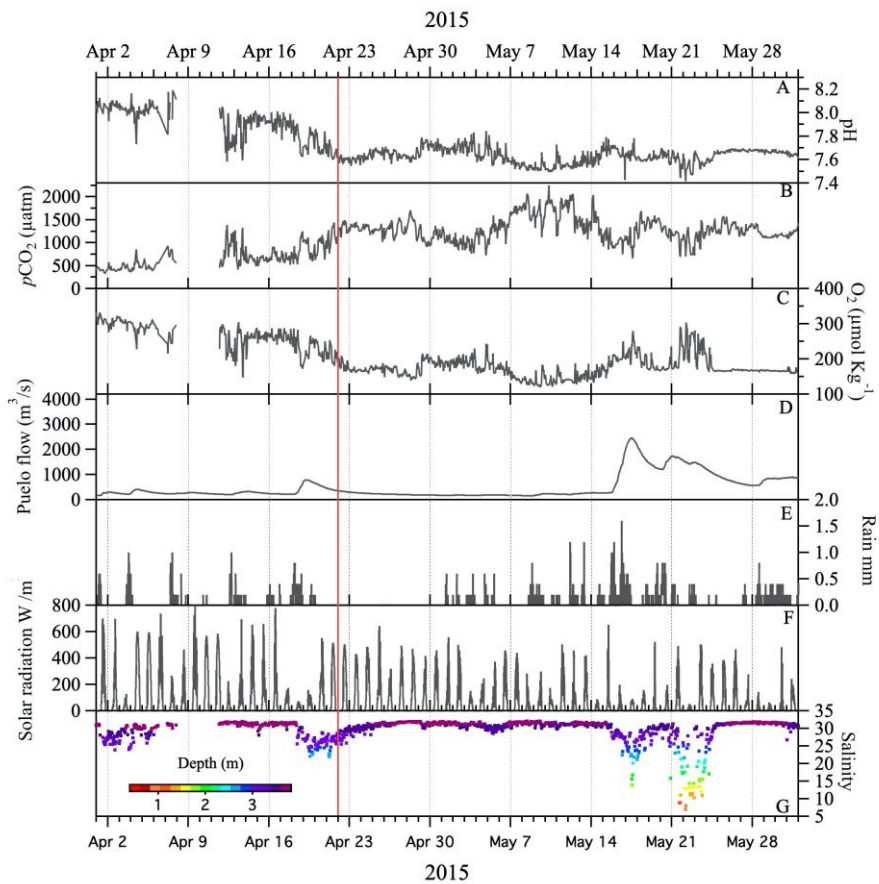


Figure 2. A Calbuco volcano ash plume 6 May 2015. B Reloncaví Fjord water with atypical high turbidity due to the ash loading, Cochamó town 6 May 2015. C Ash cloud visible on MODIS Aqua satellite from the NASA Earth Observatory, 23 April 2015 (<http://earthobservatory.nasa.gov/NaturalHazards/view.php?id=85767&eoan=home&eoci=nh>). The highlighted box in C corresponds to Fig. 1 C.

**Formatted:** Font color: Black

**Formatted:** Normal, Border: Top: (No border), Bottom: (No border), Left: (No border), Right: (No border), Between : (No border), Tab stops: 3.25", Centered + 6.5", Right



374

20  
20

Formatted: Font color: Black

Formatted: Normal, Border: Top: (No border), Bottom: (No border), Left: (No border), Right: (No border), Between : (No border), Tab stops: 3.25", Centered + 6.5", Right

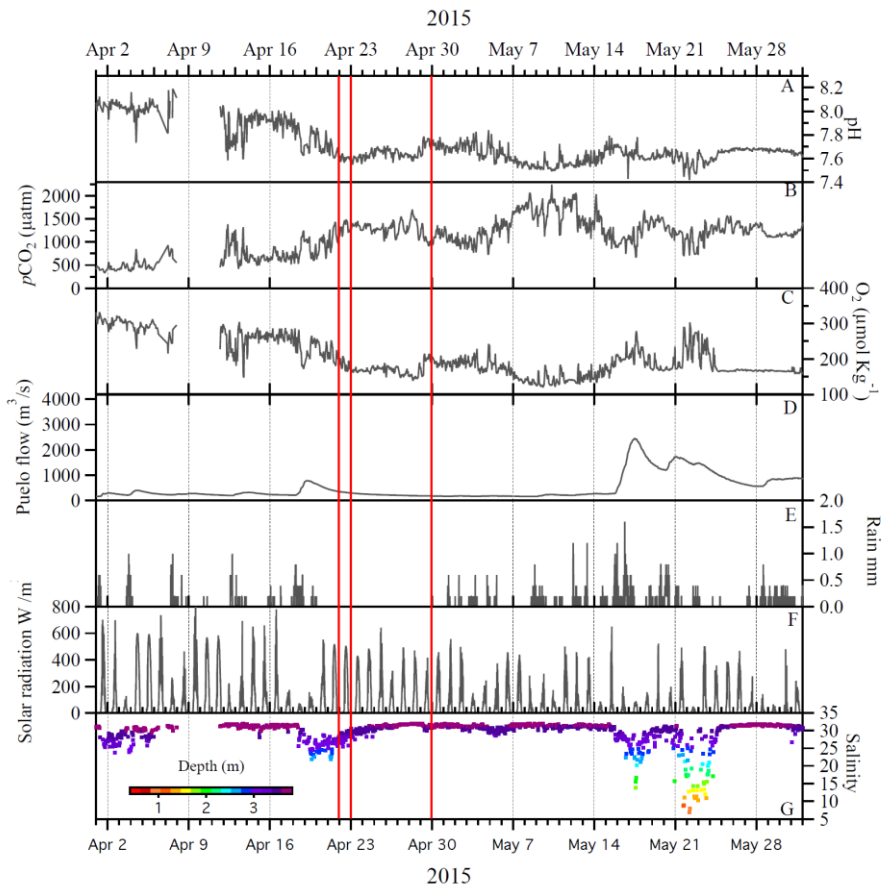


Figure 3. Continuous data from the Reloncaví Fjord mooring and nearby hydrological and weather stations for April-May 2015. The vertical red lines mark the eruption dates. All locations are marked in Fig 1. Carbonate chemistry and salinity data from Vergara-Jara et al., (2019). Wind and tidal mixing caused small changes in the depth of the sensors which are shown alongside the salinity data.

Formatted: Font color: Black

Formatted: Normal, Border: Top: (No border), Bottom: (No border), Left: (No border), Right: (No border), Between : (No border), Tab stops: 3.25", Centered + 6.5", Right

Carbonate chemistry data from the Reloncaví Fjord mooring demonstrated that pH declined and pCO<sub>2</sub> increased in the week prior to the first eruption (22 April, Fig. 3). Oxygen and pH reached a minimum and pCO<sub>2</sub> a maximum during the time period ~~May-7-14~~ May, which indicates a state of high respiration. In this stratified environment, the brackish fjord surface layer has generally low pH, high pCO<sub>2</sub> with seasonal changes in salinity and respiration leading to a large annual range of pCO<sub>2</sub> and pH (Vergara-Jara et al., 2019). The depth of the sensors varied temporally due to changes in tides and river flow. This accounts for some of the variation in measured salinity due to the strong salinity gradient with depth in the brackish surface waters (Fig. 3). Any changes to pCO<sub>2</sub> or pH occurring as a direct result of the ~~eruption~~ eruptions, or associated ash deposition, are therefore challenging to distinguish from background variation due to short-term (intra-day) or seasonal shifts in the carbonate system which are pronounced in this dynamic and strongly freshwater influenced environment (Fig. 3). Freshwater discharge from the Puelo increased sharply from 16 ~~May-16~~ which is an annually recurring event (González et al., 2010).

### 3.2 Phytoplankton in Reloncaví fjord post-eruption

**Formatted:** Font color: Black

**Formatted:** Normal, Border: Top: (No border), Bottom: (No border), Left: (No border), Right: (No border), Between : (No border), Tab stops: 3.25", Centered + 6.5", Right

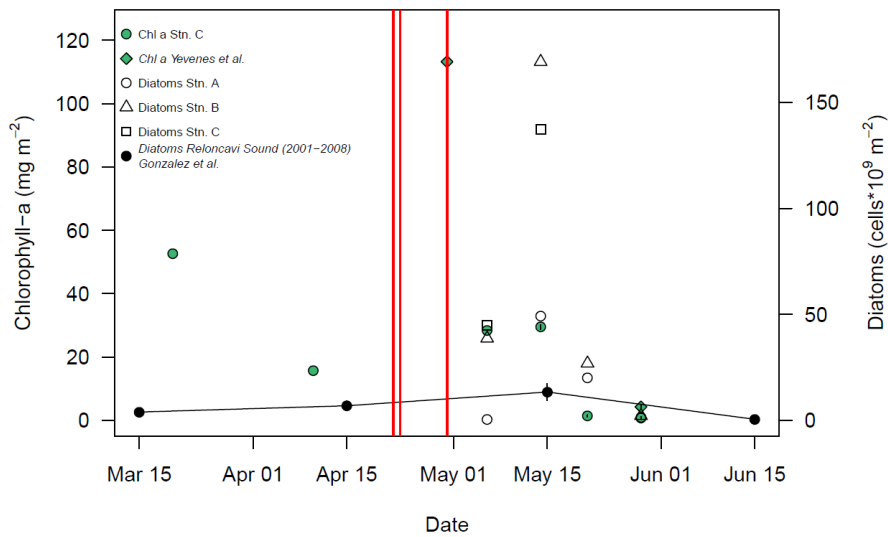
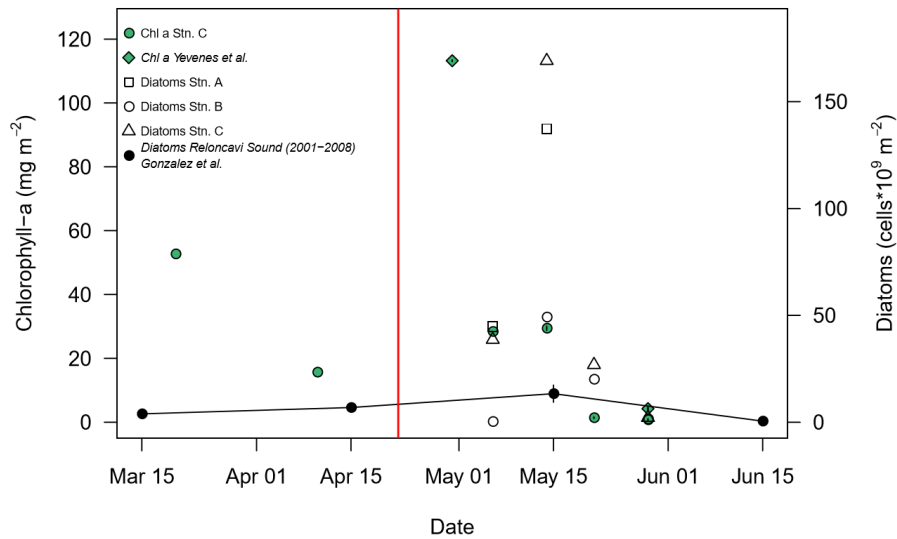


Figure 4. Changes in integrated (0-15 m) diatom abundance and chlorophyll-a for Reloncaví Fjord in April-May 2015. Locations as per Fig. 1, the eruption date (22 April) is dates are marked with red lines. Historical diatom data from Reloncaví Sound (2001-2008, integrated

Formatted: Font color: Black

Formatted: Normal, Border: Top: (No border), Bottom: (No border), Left: (No border), Right: (No border), Between : (No border), Tab stops: 3.25", Centered + 6.5", Right

to 10 m depth, mean  $\pm$  standard error (González et al., 2010) and additional chlorophyll data from 2015 ('Station 3' from Yevenes et al., 2019, approximately corresponding to Station C herein) are also shown.

) and additional chlorophyll data from 2015 ('Station 3' from Yevenes et al., 2019, approximately corresponding to Station C herein) are also shown.

Phytoplankton abundances observed in May 2015 within Reloncaví Fjord were assessed by diatom cell counts and chlorophyll-a concentrations (Sup. Table 3) and were proportionate to, or higher than, those previously observed in the region (Fig. 4). When comparing observations to prior data from González et al., (2010) it should be noted that there is a slight depth discrepancy (earlier work was integrated to 10 m depth rather than 15 m herein). Yet as the phytoplankton bloom is overwhelmingly present within the upper 10 m these data do provide a useful comparison. Diatom abundance integrated to 15 m depth peaked at Stations AB and C around 14<sup>th</sup> May, with notably lower abundances at the more freshwater influenced innermost station BA (Fig. 4), located at a mid fjord site between the 3 major river outflows. The highest measured chlorophyll-a concentrations were on 30<sup>th</sup> April at Station C, including two nearby measurements from Yevenes et al., (2019), then chlorophyll-a values declined to much lower concentrations in late May which is expected from patterns in regional primary production (González et al., 2010). No measurements were available for 10-30 April 2015 (Fig. 4) and thus it is not possible to determine the timing of the onset of the austral autumn phytoplankton bloom with respect to the volcanic eruption eruptions from the available chlorophyll-a or diatom data. Within this

Field Code Changed

Formatted: Font color: Black

Formatted: Normal, Border: Top: (No border), Bottom: (No border), Left: (No border), Right: (No border), Between : (No border), Tab stops: 3.25", Centered + 6.5", Right



time period, the mooring at Station C (Fig. 3) however did record a modest increase in pH and O<sub>2</sub> from 28-29 April, during a time period when river discharge and salinity were stable, which could be indicative of the autumn phytoplankton bloom onset.

### 3.3 Total alkalinity and macronutrients in leach experiments

Size analysis of the collected ash determined a mean particle diameter of 339  $\mu\text{m}$ . Small ash-particles ( $<63 \mu\text{m}$ ) resulted in minor, or no significant, changes to A<sub>T</sub> in brackish fjord waters (Fig. 5). With ~~large~~<sup>larger</sup> ash-particles ( ~~$\approx 1.0 \text{ mm}$~~ <sup>(250-1000  $\mu\text{m}$ )</sup>) no effect was evident. Conversely, a leaching experiment with de-ionized water showed a small increase in A<sub>T</sub> (Fig. 5) for both size fractions. By increasing the A<sub>T</sub> of freshwater, ash would act to increase the buffering capacity of river outflow into a typically weak carbonate system like the Reloncaví Fjord (Vergara-Jara et al., 2019). However, the absolute change in A<sub>T</sub> was relatively small despite the large ash loading used in all incubations ( $< 20 \mu\text{mol kg}^{-1}$  A<sub>T</sub> for ash loading  $> 4 \text{ g L}^{-1}$ ) and therefore it is expected that the direct effect of ash on A<sub>T</sub> in situ was limited. Other effects on carbonate chemistry may however arise due to ash moderating the timing and intensity of primary production and thus biological pCO<sub>2</sub> drawdown.

Formatted: Font color: Black

Formatted: Normal, Border: Top: (No border), Bottom: (No border), Left: (No border), Right: (No border), Between : (No border), Tab stops: 3.25", Centered + 6.5", Right

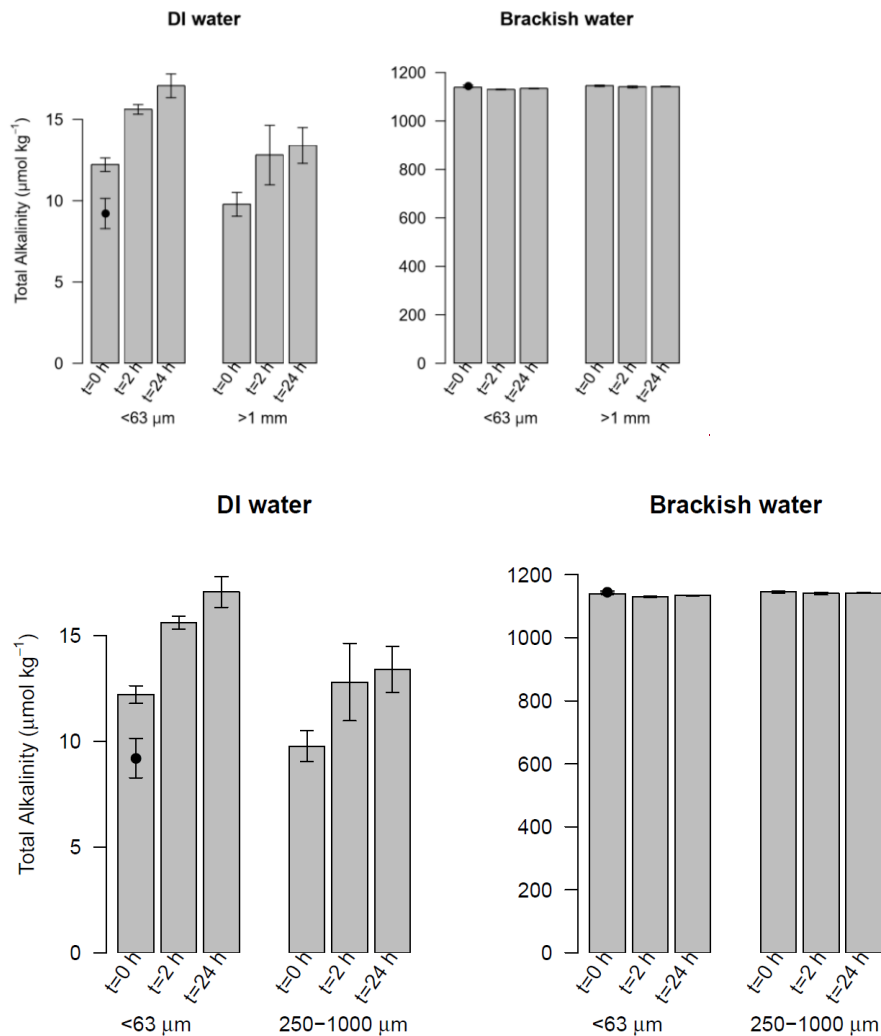


Figure 5. Total alkalinity released after leaching 4.5 g L<sup>-1</sup> ash of two size fractions (<63 μm and >1.0 mm) in de-ionized water (DI water) and brackish water. T<sub>0</sub>= 'time zero', measured after one minute of mixing, T<sub>2H</sub>= after two hours of mixing, T<sub>24H</sub>= after 24 hours of mixing. n=4 for all treatments (mean ± standard deviation plotted). The initial (pre-

Formatted: Font color: Black

Formatted: Normal, Border: Top: (No border), Bottom: (No border), Left: (No border), Right: (No border), Between : (No border), Tab stops: 3.25", Centered + 6.5", Right

ash addition) alkalinity is marked by a black dot superimposed on the left  $T_0$ . Source data is provided in Supplementary Table 4.

~~Ion chromatography results for Na, K, Ca, F, Cl,  $\text{NO}_3^-$  and  $\text{SO}_4^{2-}$  showed that in the presence of smaller ash size particles, ion inputs were generally higher. The leaching from ash components into de-ionized water occurred almost instantly with limited, or no increases in leached concentrations observed between 0, 2 and 24 h (Table 2). For larger particles there was less release of most ions. In the case of Ca and  $\text{SO}_4^{2-}$  a more gradual leaching effect was apparent (Table 2). The concentrations of  $\text{NO}_3^-$  and  $\text{NH}_4^+$  were generally below detection suggesting that ash was a minor source of these nutrients into solution. These observations are consistent with the trends in prior work using a range of volcanic ash and incubation conditions (Delmelle et al., 2007; Duggen et al., 2010; Witham et al., 2005).~~

Ion chromatography results for  $\text{Na}^+$ ,  $\text{K}^+$ ,  $\text{Ca}^{2+}$ ,  $\text{F}^-$ ,  $\text{Cl}^-$ ,  $\text{NO}_3^-$  and  $\text{SO}_4^{2-}$  showed that in the presence of smaller ash size particles, ion inputs were generally higher (Table 2) as has been reported previously (Jones and Gislason, 2008; Óskarsson, 1980; Rubin et al., 1994). The leaching from ash components into de-ionized water occurred almost instantly with limited, or no increases in leached concentrations observed between 0, 2 and 24 h (Table 2). For larger particles there was less release of most ions. In the case of  $\text{Ca}^{2+}$  and  $\text{SO}_4^{2-}$  a more gradual leaching effect was apparent (Table 2). The concentrations of  $\text{NO}_3^-$  and  $\text{NH}_4^+$  were generally below detection suggesting that ash was a minor source of fixed-nitrogen into solution. These observations are consistent with the trends in prior work using a range of volcanic ash and incubation conditions (Duggen et al., 2010; Witham et al., 2005). Major ion analysis was

**Formatted:** Font color: Black

**Formatted:** Normal, Border: Top: (No border), Bottom: (No border), Left: (No border), Right: (No border), Between : (No border), Tab stops: 3.25", Centered + 6.5", Right

only conducted in de-ionized water as no significant changes would be observable for most of these ions in brackish or saline waters under the same conditions.

	Time [h]	Na <sup>+</sup>	K <sup>+</sup>	Ca <sup>2+</sup>	FF <sup>-</sup>	Cl <sup>-</sup>	SO <sub>4</sub> <sup>2-</sup>	NO <sub>3</sub> <sup>-</sup>	NH <sub>4</sub> <sup>+</sup>
Detection limit		0.17	0.43	0.30	0.28	1.31	1.64	0.34	0.13
Proced. Blank		b.d.	b.d.	0.39	b.d.	b.d.	b.d.	b.d.	b.d.
>1.0 mm 250-1000 µm [µmol/l]	0.1	3.4 (2.8)	0.83 (0.3)	18.3 (3.3)	0.16 (0.05)	3.7 (1.9)	3.7 (2.2)	b.d.	0.15 (0.2)
	2	5.1 (2.0)	1.0 (0.2)	18.5 (4.5)	0.21 (0.08)	4.4 (1.6)	4.9 (2.0)	b.d.	0.38 (0.4)
	24	7.3 (0.1)	1.4 (0.2)	23.4 (3.2)	0.52 (0.18)	5.7 (0.5)	8.3 (2.1)	b.d.	b.d.
<63 µm [µmol/l]	0.1	16.2 (12.7)	3.2 (0.3)	25.1 (5.4)	0.29 (0.0)	17.1 (13.6)	13.5 (1.3)	0.53 (0.2)	1.70 (1.1)
	2	16.7 (1.0)	3.8 (0.1)	31.8 (2.7)	0.63 (0.2)	15.2 (0.9)	19.0 (0.3)	b.d.	0.52 (1.0)
	24	17.3 (0.8)	3.9 (0.3)	33.8 (3.3)	0.69 (0.3)	14.6 (1.0)	18.8 (0.5)	b.d.	1.32 (2.6)
<63 µm [µmol/g ash]	24	3.84	0.87	7.50	0.15	3.25	4.18	0.048	0.29
	Range (lit.)	1.5-84.3	0.1-5.4	0.6-589	0.1-9	2-92.9	1-554	0-6.4	0.3-0.6

Formatted Table

Table 2. Major ion and macronutrient concentrations in µmol/l leached from the two size fractions of ash (< 63 µm and >1.0 mm) into deionized water (b.d. = below detection). Shown are mean, with standard deviation in parentheses (n=4). Also shown are mass normalized values [µmol/g ash], and a comparison to the range of values reported by Jones and Gislason, (2008). 250-1000 µm) into deionized water (b.d. = below detection). Shown are mean, with standard deviation in parentheses (n=4). Also shown are mass normalized values [µmol/g ash], and a comparison to the range of values reported by Jones and Gislason (2008).

### 3.4 Trace elements in leach experiments

Release of nanomolar concentrations of dissolved Fe and Mn was evident when ash was re-suspended in aged seawater for 10 minutes (Fig. 6). The net release of dissolved metals proceeded with varying relationships with ash loading over the applied gradient (0.1–62.50 mg L<sup>-1</sup>). Dissolved Mn, Pb, Cu and Co release exhibited significant (p < 0.05) positive

Formatted: Font color: Black

Formatted: Normal, Border: Top: (No border), Bottom: (No border), Left: (No border), Right: (No border), Between : (No border), Tab stops: 3.25", Centered + 6.5", Right

relationships with ash loading, with Mn and Cu exhibiting the most linear behavior ( $R^2$  0.99 and 0.83, respectively). Dissolved Fe, Cd and Ni showed no significant relationships with ash loading over the applied range. The initial concentration of metals in South Atlantic seawater should however also be considered when interpreting the trends. The magnitude of changes in Cd and Ni concentrations were smallest relative to both the initial concentration and the standard deviation on the initial concentration ( $0.38 \pm 0.04$  nM Cd and  $6.58 \pm 0.76$  nM Ni, respectively). It thus would be difficult to extract a clear relationship irrespective of their chemical behavior. For other elements, (Fe, Co and Pb), non-linearity between ash addition and trace metal concentrations, and some negative changes in concentrations, both likely reflect scavenging of metal ions onto ash particle surfaces (Rogan et al., 2016). Fe, Co and Pb are all scavenged type elements and so increasing the surface area of ash present may affect the net change in metal concentration. The divergence between the behaviour of Mn and Fe, with Mn showing a stronger relationship with ash loading, supports the hypothesis of Mendez et al., (2010), that the release of dissolved Mn from aerosols into seawater depends primarily on ash Mn availability whereas the release of dissolved Fe is more dependent on the nature of organic material present in solution.

**Formatted:** Font color: Black

**Formatted:** Normal, Border: Top: (No border), Bottom: (No border), Left: (No border), Right: (No border), Between : (No border), Tab stops: 3.25", Centered + 6.5", Right

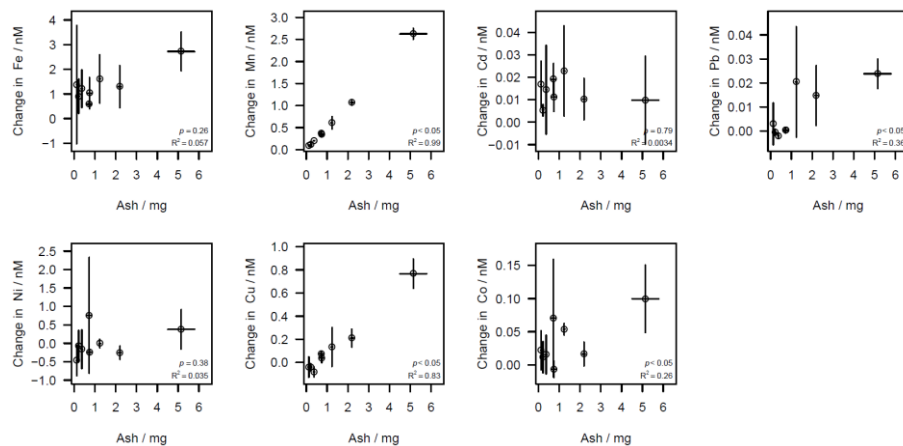


Figure 6. Change in trace metal concentrations after varying ash addition to 100 ml South Atlantic seawater for a 10-minute leach duration at room temperature. Initial (mean  $\pm$  standard deviation) dissolved trace metal concentrations - deducted from the final concentrations to calculate the change as a result of ash addition - were  $0.98 \pm 0.03$  nM Fe,  $0.38 \pm 0.04$  nM Cd,  $13 \pm 2$  pM Pb,  $6.58 \pm 0.76$  nM Ni,  $0.84 \pm 0.07$  nM Cu,  $145 \pm 9$  pM Co,  $0.72 \pm 0.05$  nM Mn. Error bars are standard deviations from triplicate treatments with similar ash loadings. p values and R<sup>2</sup> for a linear regression are annotated. [Source data is provided in Supplementary Table 5. The same data with individual replicates is shown in Supplementary Figure 1.](#)

Formatted: Font color: Black

Formatted: Normal, Border: Top: (No border), Bottom: (No border), Left: (No border), Right: (No border), Between : (No border), Tab stops: 3.25", Centered + 6.5", Right

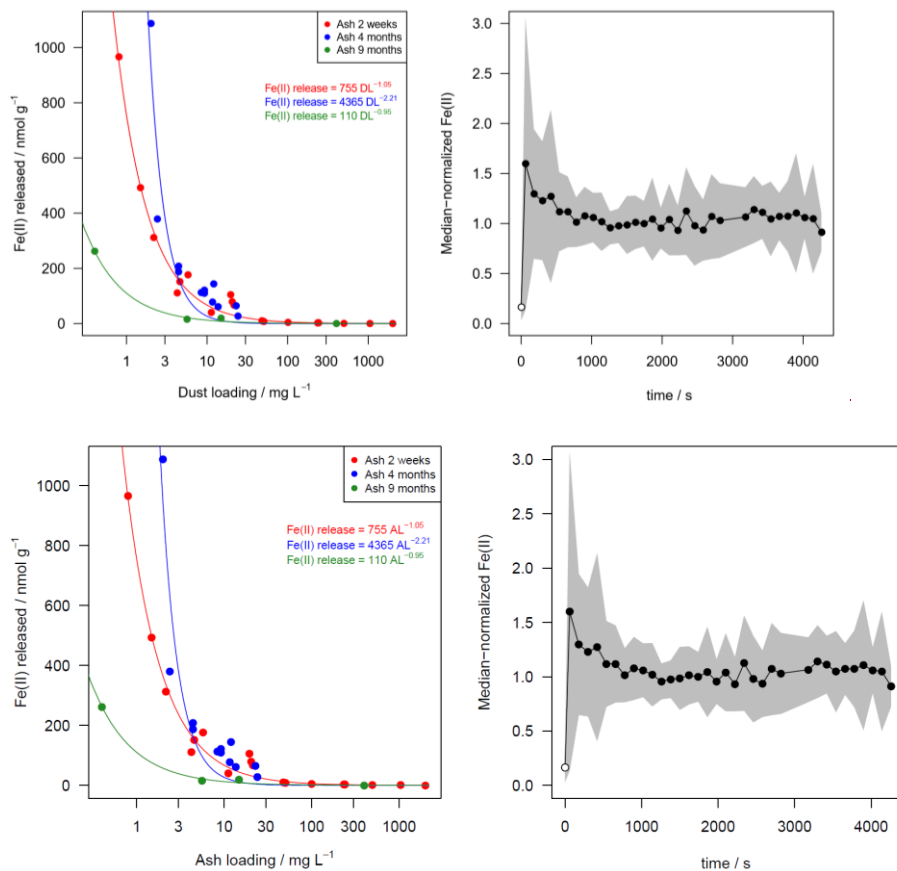


Figure 7. Fe(II) release from Calbuco ash into seawater. Mean Fe(II) released into South Atlantic seawater over a 30 minute leach at 5-7°C (left). The same batch of Calbuco ash was subsampled and used to conduct experiments on 3 occasions after the 2015 eruption (2 weeks, 4 months and 9 months since ash collection). The 30 minutelines are power law fits, with associated equations shown in the legend. The 3 time-series of Fe(II) concentrations following ash addition areis considered collectively by normalizing the measured concentrations (right), such that 1.0 represents the median Fe(II) concentration measured in

Formatted: Font color: Black

Formatted: Normal, Border: Top: (No border), Bottom: (No border), Left: (No border), Right: (No border), Between : (No border), Tab stops: 3.25", Centered + 6.5", Right

each experiment ~~2-30 minutes after ash addition.~~ All experiments were conducted for at least 30 minutes, those conducted with 4/9 months old ash were extended for 1 hour. The black line shows the mean response over 34 leach experiments with varying ash loading, the shaded area shows  $\pm 1$  standard deviation. The initial Fe(II) concentration (pre-ash addition at 0 s) in all cases was below detection and thus the detection limit is plotted at 0 s (open circle). Source data is provided in Supplementary Table 2.

In addition to the release of dFe in solution, which generally exists as Fe(III) species in oxic seawater (Gledhill and Buck, 2012), the release of Fe(II) was evident on a similar timescale when cold (5-7°C) aged S Atlantic seawater was used as leachate (Fig. 7). The half-life of Fe(II) decreases more than tenfold as temperature is increased from 5 to 25°C, leading to Fe(II) decay on timescales shorter than the time required for analysis (approximately 60 s for solution to enter the flow injection apparatus, mix with reagent and generate a peak) (Santana-Casiano et al., 2005). Elevated Fe(II) concentrations ~~of up to 4, (mean 0.8 nM Fe(II),~~ Sup. Table 2) were evident at this temperature (5-7°C), which represents an intermediate sea surface temperature for the high latitude ocean. A sharp decline in Fe(II) dissolution efficiency with increasing ash load was also evident (Fig. 7). Both the highest Fe(II) concentration and the highest net release of Fe(II) were observed at the lowest ash loading (Fig. ~~77 and Sup. Fig. 2~~). Fe(II) concentration following dust addition into seawater was possibly reduced when the same experimental leaches with ash were repeated 9 months after the initial experiment. The first leaches were conducted ~2 weeks after ash collection. The absence of a clear change between 2 weeks and 4 months precludes an accurate assessment of the rate at which Fe(II) solubility may have decreased.

Formatted: Font color: Black

Formatted: Normal, Border: Top: (No border), Bottom: (No border), Left: (No border), Right: (No border), Between : (No border), Tab stops: 3.25", Centered + 6.5", Right



As Fe(II) concentrations were measured continuously using flow injection analysis, the temporal development of Fe(II) concentration after ash addition to cold seawater can also be shown (Fig. 7). Considering the set of leach experiments collectively, all ash additions were characterized by a sharp increase in Fe(II) concentrations in the first minute after ash addition into seawater. This was typically followed by a decline and then a relatively stable Fe(II) concentration (Fig. 7).

### 3.5 Satellite observations

Five-day composite images of atmospheric aerosol loading (UV aerosol index) ~~indicated two main volcanic eruption plume trajectories, which largely represents strongly UV-absorbing dust, Torres et al., 2007)~~ indicated two main volcanic eruption plume trajectories following the major eruptions on 22 and 23 April: (i) northwards over the Pacific, and (ii) northeast over the Atlantic. Daily resolved time series were constructed for regions in the Atlantic and Pacific with elevated atmospheric aerosol loading (UV Aerosol Index ~2 a.u.; Fig. 8). The Pacific time series indicated a pronounced peak in aerosol index followed by chlorophyll-a one day later. A control region to the south of the ash-impacted Pacific region showed no clear changes in chlorophyll-a matching that observed in the higher UV aerosol index region to the north— (Sup. Fig. 3).

Conversely, in the Atlantic, where the background chlorophyll-a concentration was higher throughout the time period of interest, the main area with enhanced aerosol index was not clearly associated with a change in chlorophyll-a dynamics on a timescale comparable to that observed following other volcanic ash fertilized events (Fig. 8). In a smaller ash impacted

Formatted: Font color: Black

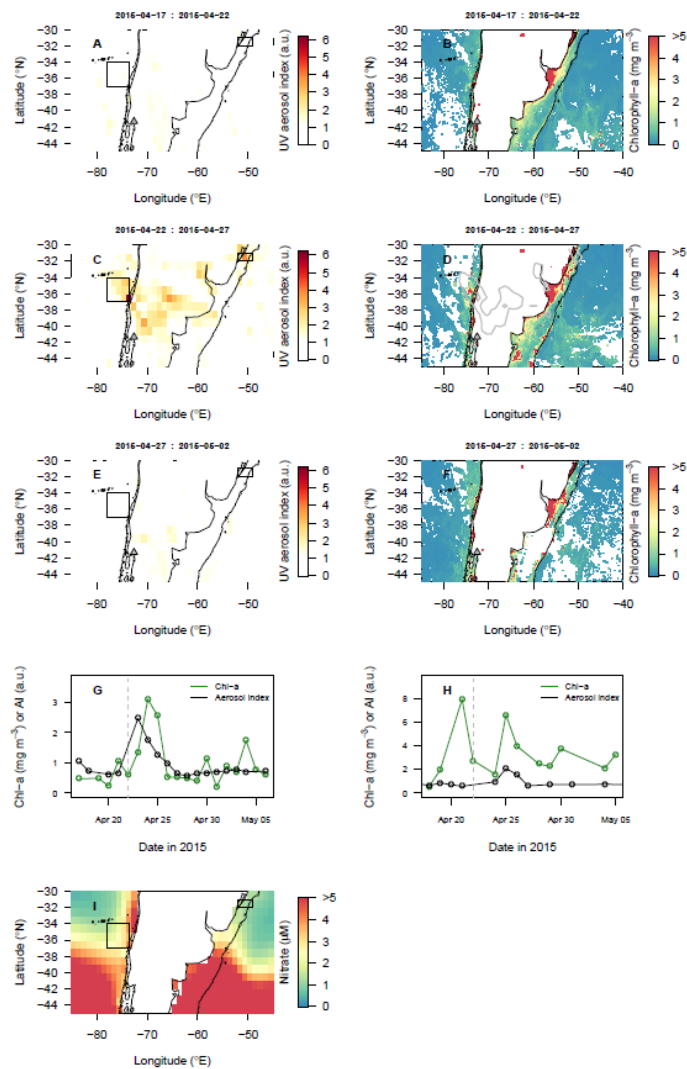
Formatted: Normal, Border: Top: (No border), Bottom: (No border), Left: (No border), Right: (No border), Between : (No border), Tab stops: 3.25", Centered + 6.5", Right

area to the south of the Rio de la Plata (Sup. Fig. 3), where nitrate levels are expected to be higher than to the north and Fe levels also expected to be elevated due its location on the continental shelf, a chlorophyll-a peak was evident 7 days after the UV aerosol peak. However, this was not well constrained due to poor satellite coverage in the period after the eruption.

Prior eruptions have been attributed with driving time periods of enhanced regional marine primary production beginning 3-5 days post-eruption (Hamme et al., 2010; Langmann et al., 2010; Lin et al., 2011) and bottle experiments showing positive chlorophyll changes in response to ash addition are typically significant compared to controls within 1-4 days following ash addition (~~Browning et al., 2014; Duggen et al., 2007; Mélançon et al., 2014~~)(Browning et al., 2014; Duggen et al., 2007; Mélançon et al., 2014).

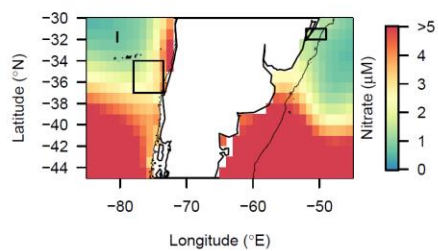
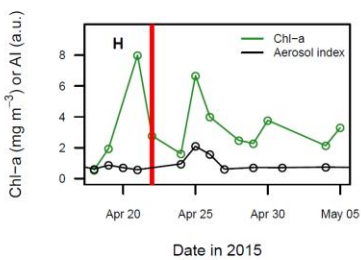
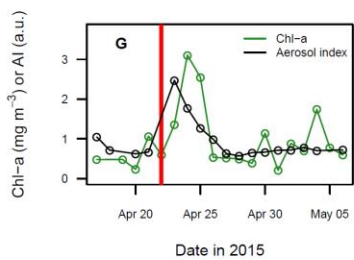
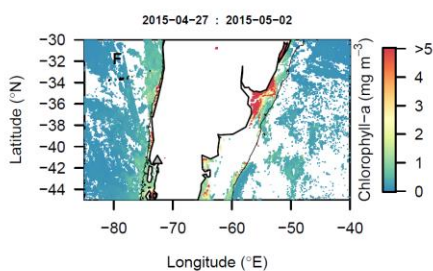
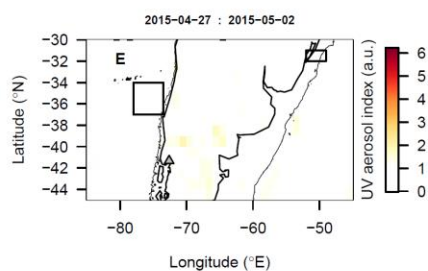
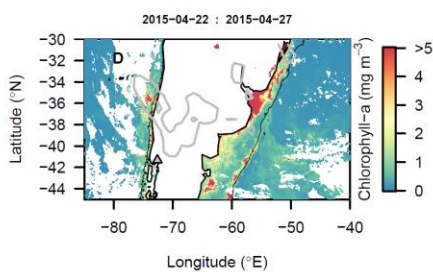
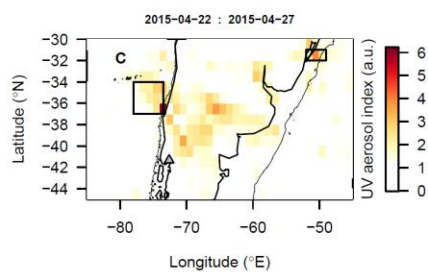
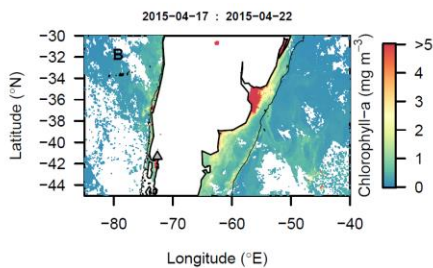
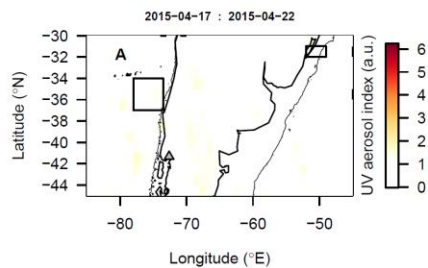
**Formatted:** Font color: Black

**Formatted:** Normal, Border: Top: (No border), Bottom: (No border), Left: (No border), Right: (No border), Between : (No border), Tab stops: 3.25", Centered + 6.5", Right



**Formatted:** Font color: Black

**Formatted:** Normal, Border: Top: (No border), Bottom: (No border), Left: (No border), Right: (No border), Between : (No border), Tab stops: 3.25", Centered + 6.5", Right



Formatted: Font color: Black

Formatted: Normal, Border: Top: (No border), Bottom: (No border), Left: (No border), Right: (No border), Between : (No border), Tab stops: 3.25", Centered + 6.5", Right

Figure 8. Potential biological impact of the 2015 Calbuco eruption observed via satellite remote sensing. (A-F) Spatial maps showing the distribution of ash in the atmosphere (UV Aerosol Index) and corresponding images of chlorophyll-a. Images were composited over 5-day periods. Grey lines in chlorophyll maps corresponds to the UV Aerosol index = 2 a.u. contour. (G, H) Time series of UV Aerosol Index and chlorophyll-a for regions of the Pacific (G) and Atlantic (H) identified by boxes in maps. ~~DashedRed~~ vertical lines (22 April) indicate the first eruption date. (I) Mean World Ocean Atlas surface NO<sub>3</sub> concentrations. Thin black lines indicate the 500 m bathymetric depth contour.

## 4 Discussion

### 4.1 Local drivers of 2015 bloom dynamics in Reloncaví Fjord

The north Patagonian archipelago and fjord region have a seasonal phytoplankton bloom cycle with peaks in productivity occurring in May and October (austral autumn and spring) and the lowest productivity consistently in June (austral winter) (González et al., 2010). Diatoms normally dominate the phytoplankton community during the productive period due to high light availability and high silicic acid supply, both of which are influenced by freshwater runoff (González et al., 2010; Torres et al., 2014). The austral fall season, encompassing the April-May 2015 ash ~~fall~~deposition events, is therefore expected to have a high phytoplankton biomass (Iriarte et al., 2007; León-Muñoz et al., 2018) which terminates abruptly with decreasing light availability in austral winter (González et al., 2010).

Whilst not directly comparable, the magnitude of the 2015 bloom in terms of diatom abundance (Fig. 4) was more intense than that reported in Reloncaví Sound 2001-2008. With

Field Code Changed

Formatted: Font color: Black

Formatted: Normal, Border: Top: (No border), Bottom: (No border), Left: (No border), Right: (No border), Between : (No border), Tab stops: 3.25", Centered + 6.5", Right

respect to the timing of the phytoplankton bloom, the low diatom abundances and chlorophyll-a concentrations at the end of May (Fig. 4) are consistent with prior observations of sharp declines in primary production moving into June (González et al., 2010). Peaks in diatom abundance were measured at two stations on ~~14th~~<sup>14</sup> May one week after the third (small) eruptive pulse, and measured chlorophyll-a concentrations were highest close to Station C on 30 April (Fig. 4). The high-resolution pH and O<sub>2</sub> data collected at Station C from mooring data is consistent with an intense phytoplankton bloom between ~29 April and 7 May (Fig. 3) indicated by a shift to slightly higher pH and O<sub>2</sub> during this time period when river flow into the fjord was stable.

Without a direct measure of ash deposition per unit area in the fjord, turbidity, or higher resolution chlorophyll/diatom data, it is challenging to unambiguously determine the extent to which the austral autumn phytoplankton bloom was affected by volcanic activity. The high abundance of diatoms at two of three stations sampled could have resulted from ash fertilization. Yet if this was the case, it is not clear which nutrient was responsible for this fertilization, why the bloom initiation occurred about one week after the third eruptive pulse (several weeks after the main eruption events) and to what extent the timing was coincidental given that productivity normally peaks in May. Reloncaví Fjord was to the south of the dominant ash deposition from the 22 and 23 April eruptions (Romero et al., 2016). ~~Both runoff and rainfall were vectors by which ash was deposited in the fjord, which and thus ash was delivered by a mixture of vectors including runoff and rainfall. The Petrohue river basin was particularly severely affected by ash with deposition of up to 50 cm ash in places. This~~ complicates the interpretation of the time series provided by high resolution data (Fig. 3).

Formatted: Font color: Black

Formatted: Normal, Border: Top: (No border), Bottom: (No border), Left: (No border), Right: (No border), Between : (No border), Tab stops: 3.25", Centered + 6.5", Right

With incident light also highly variable over the time series (Fig. 3F), there are clearly several factors, other than volcanic ash deposition, which will have exerted some influence on diatom and chlorophyll-a abundance throughout May 2015.

Primary production in the Reloncaví region is thought to be limited by light availability rather than macronutrient availability (González et al., 2010). Whilst micronutrient availability relative to phytoplankton demand has not been extensively assessed in this fjord, with such higher riverine inputs across the region- which are normally a large source of dissolved trace elements into coastal waters (e.g. Boyle et al., 1977)- limitation of phytoplankton growth by Fe, or another micronutrient, seems implausible. Reported Fe concentrations determined by a diffusive gel technique in Reloncaví Fjord in October 2006 were relatively high; 46-530 nM (Ahumada et al., 2011). Similarly, reported dFe concentrations in the adjacent Comau Fjord at higher salinity are generally in the nanomolar range and remain >2 nM even under post-bloom conditions which suggests dFe is not a limiting factor for phytoplankton growth (Hopwood et al., 2020; Sanchez et al., 2019).

Silicic acid availability could have been increased by ash deposition. Whilst not quantified herein, an increase in silicic acid availability from ash in a region where silicic acid was sub-optimal for diatom growth could plausibly explain higher than usual diatom abundance (Siringan et al., 2018). Silicic acid concentrations were indeed high (up to ~~80~~118  $\mu\text{M}$ ) in Reloncaví Fjord surface waters ~~in May 2015~~>30  $\mu\text{M}$  at 15 m depth (salinity 33.4) ~~(Yevenes et al., 2019), however concentrations in excess of (Vergara-Jara et al., 2019; Yevenes et al., 2019).~~However concentrations >30  $\mu\text{M}$  are typical during periods of high

Formatted: Font color: Black

Formatted: Normal, Border: Top: (No border), Bottom: (No border), Left: (No border), Right: (No border), Between : (No border), Tab stops: 3.25", Centered + 6.5", Right

runoff and accordingly are not thought to limit primary production or diatom growth [in this area](#) (González et al., 2010). The  $\text{Si(OH)}_4\text{:NO}_3$  ratio in Reloncaví Fjord and downstream Reloncaví Sound also indicates an excess of  $\text{Si(OH)}_4$ , with ratios of approximately 2:1 observed in fjord surface waters throughout the year (González et al., 2010; Yevenes et al., 2019). For comparison, the ratio of Si:N for diatom nutrient uptake is 15:16 (Brzezinski, 1985). Furthermore, experimental incubations making additions of macronutrients to fjord waters in Reloncaví and adjacent fjords, have found strong responses of phytoplankton to additions of silicic acid only when  $\text{Si(OH)}_4$  and  $\text{NO}_3$  were added in combination, further corroborating the hypothesis that an excess of silicic acid is normally present in surface waters of these fjord systems (Labbé-Ibáñez et al., 2015). It is therefore doubtful that changes in nutrient availability from ash alone could explain such high diatom abundances in mid-May.

Alternative reasons for high diatom abundances in the absence of a chemical fertilization effect are plausible and could include, for example, ash having reduced zooplankton abundance or virus activity in the fjord, thus facilitating higher diatom abundance than would otherwise have been observed by decreasing diatom mortality rates in an environment where nutrients were replete. The role of volcanic ash in driving such short-term ecological shifts in the marine environment is almost entirely unstudied (Weinbauer et al., 2017). However, volcanic ash deposition of  $7 \text{ mg L}^{-1}$  in lakes within this region during the 2011 Puyehue-Cordón Caulle eruption was reported to increase post-deposition phytoplankton biomass and decrease copepod and cladoceran biomass (Wolinski et al., 2013). The proposed mechanism was ash particle ingestion negatively affecting zooplankton, and ash-shading positively

**Formatted:** Font color: Black

**Formatted:** Normal, Border: Top: (No border), Bottom: (No border), Left: (No border), Right: (No border), Between : (No border), Tab stops: 3.25", Centered + 6.5", Right



affecting phytoplankton via reduced photoinhibition (Balseiro et al., 2014; Wolinski et al., 2013).

Field Code Changed

Considering the more modest peak in diatom abundance at the most strongly ash affected station (Station A, Fig. 4) and the timing of the peak diatom abundance 3 weeks after the main eruption, it is clear that the interaction between ash and phytoplankton in the Reloncaví Fjord was more complex than the simple Fe-fertilization proposed for the SE Pacific (Fig. 8g). In the absence of an immediate diatom fertilization effect from Fe or silicic acid, we hypothesize that any change in phytoplankton bloom dynamics within Reloncaví Fjord was mainly a ‘top-down’ effect driven by the physical interaction of ash and different ecological groups in a nutrient replete environment, rather than a ‘bottom-up’ effect driven by alleviation of nutrient-limitation from ash dissolution.

#### 4.2 Volcanic ash as a unique source of trace elements

Formatted: English (United States)

The release of the bioessential elements Fe and Mn from ash here ranged from 53 - 1200 nmol g<sup>-1</sup> (dFe) and 48 - 71 nmol g<sup>-1</sup> (dissolved Mn), which is comparable to the rates determined in other studies under similar experimental conditions (Duggen et al., 2010). Fe(II) release was particularly efficient at ash loadings <5 mg L<sup>-1</sup> (Fig. 7). For dFe this is comparable to the rates determined in other studies under similar experimental conditions for subduction zone volcanic ash, with reported Fe-release in prior work ranging 2-570 nmol g<sup>-1</sup> (Sup. Table 1). For Mn, less prior work is available, but these values are within the 17-1300 nmol g<sup>-1</sup> range reported by Hoffmann et al., (2012). Fe(II) release was particularly efficient at ash loadings <5 mg L<sup>-1</sup> (Fig. 7), whereas dFe release was less sensitive to ash loading (Fig. 6). The timing of Fe(II) release in the first 60 s of incubations suggests a fast dissolution

Formatted: English (United States)

Formatted: Font color: Black

Formatted: Normal, Border: Top: (No border), Bottom: (No border), Left: (No border), Right: (No border), Between : (No border), Tab stops: 3.25", Centered + 6.5", Right

process. Fe(II) is short lived in oxic surface seawater with an observed half-life of only 10-20 minutes even in the Southern Ocean where cold surface waters slow Fe(II) oxidation (Sarthou et al., 2011). Yet, relative to Fe(III), Fe(II) is also more soluble and, from an energetic perspective, expected to be more bioaccessible to cellular uptake (Sunda et al., 2001). Whilst it is known that the vast majority of dFe leached from ash into seawater tends to occur in the first minutes of ash addition (Duggen et al., 2007; Jones and Gislason, 2008) and this could be consistent with rapid dissolution of highly soluble phases on ash surfaces, we note that there is not yet conclusive evidence concerning the precise origin of this dFe pulse. Fe(II) salts may be present on the surface of ash particles (Horwell et al., 2003; Hoshyaripour et al., 2015) and thus the Fe(II) observed herein (Fig. 7) may reflect almost instantaneous release following dissolution of thin layers of salt coatings in ash surfaces (Ayris and Delmelle, 2012; Delmelle et al., 2007; Olsson et al., 2013). Alternatively Fe(II) could be released from more crystalline Fe(II) phases. Prior work, at much lower pH (pH 1 H<sub>2</sub>SO<sub>4</sub> representing conditions that ash surfaces may experience during atmospheric processing, but not in aquatic environments) suggests that short-term release of Fe(II) or Fe(III) is determined by the surface Fe(II)/Fe ratio which may differ from the bulk Fe(II)/Fe ratio due to plume processing (Maters et al., 2017). Different leaching protocols are widely recognised as a major challenge for interpreting and comparing different dissolution experiment datasets for all types of aerosols (Duggen et al., 2007; Morton et al., 2013). When Fe(II) is released into solution as a considerable fraction of the total dFe release this is particularly challenging to monitor, as Fe(II) oxidises on timescales of seconds to minutes depending on temperature, pH and O<sub>2</sub> conditions (Santana-Casiano et al., 2005). The dFe and Fe(II) leaching protocols used herein are only comparable

Formatted: English (United States)

Formatted: English (United States)

Formatted: English (United States)

Formatted: English (United States)

Formatted: English (United States)

Formatted: English (United States)

Formatted: English (United States)

Formatted: English (United States)

Formatted: English (United States)

Formatted: English (United States)

Formatted: English (United States)

Formatted: English (United States)

Formatted: English (United States)

Formatted: English (United States)

Formatted: Font color: Black

Formatted: Normal, Border: Top: (No border), Bottom: (No border), Left: (No border), Right: (No border), Between : (No border), Tab stops: 3.25", Centered + 6.5", Right

qualitatively, as the Fe(II) method using cooler seawater and larger seawater volumes was specifically designed to test for the presence of rapid Fe(II) release and to evaluate the short-term temporal trend of any such release. Yet, for rough comparative purposes, the Fe(II) released was equivalent to  $38 \pm 25\%$  (mean  $\pm$  standard deviation) of dFe released at ash loadings from 1-10 mg L<sup>-1</sup> and  $19 \pm 17\%$  of dFe for ash loadings from 10-50 mg L<sup>-1</sup>. These values are reasonably comparable to the 26% median Fe(II)/dFe fraction measured in Fe released into seawater from aerosols collected across zonal transects of the Pacific Ocean (Buck et al., 2013) suggesting that fresh Calbuco ash is roughly comparable in terms of Fe(II) lability to these environmentally processed aerosols.

#### 4.3 A potential fertilization effect in the SE Pacific

Experiments with ash suspensions have shown that ash loading has a restricted impact on satellite chlorophyll-a retrieval (Browning et al., 2015), therefore offering a means to assess the potential biological impact of the 2015 Calbuco eruption in offshore waters. We found evidence for fertilization of offshore Pacific seawaters in the studied area (Fig. 8). Following the eruption date, mean chlorophyll-a concentrations increased ~2.5 times over a broad region where elevated UV aerosol index was detected (Fig. 8G). Both the timing and location of this chlorophyll-a peak were consistent with ash fertilization, with the peak of elevated chlorophyll-a being located within the core of highest atmospheric aerosol loading, and the peak date occurring one day after the main passage of the atmospheric aerosol plume. A similar phytoplankton response timeframe was reported following ash deposition in the NE Pacific following the August 2008 Kasatochi eruption (Hamme et al., 2010) which was similarly thought to be triggered by relief of Fe-limitation (Langmann et al., 2010). At the same time, a control region to the south of the ash-impacted Pacific region showed no clear

Formatted: Font color: Black

Formatted: Normal, Border: Top: (No border), Bottom: (No border), Left: (No border), Right: (No border), Between : (No border), Tab stops: 3.25", Centered + 6.5", Right

changes in chlorophyll-a matching that observed in the higher UV aerosol index region to the north (Sup. Fig. 3).

In the SW Atlantic, two ash impacted areas are highlighted; one to the north (Fig. 8), and one to the south of the Rio de la Plata (Sup. Fig. 3). Nitrate levels are expected to be higher in the south than to the north, with Fe levels expected to be elevated across both locations as a result of their position on the continental shelf. In the area to the north of the Rio de la Plata (Fig. 8), ash deposition indicated by the UV aerosol index did not lead to such a clear corresponding change in chlorophyll-a concentrations (Fig. 8H), although with the available data it is not possible to rule out the possibility of fertilisation completely (e.g., ~~A smaller ash impacted area to the south of the Rio de la Plata, where nitrate levels are expected to be higher than to the north, but with Fe levels also expected to be elevated due its location on the continental shelf, showed a chlorophyll a peak 7 days after the UV aerosol peak (Sup. Fig. 3). However, this was not well constrained due to poor satellite coverage in the period after the eruption. Considering the dynamic spatial and temporal variation in chlorophyll within this coastal area, it is challenging to associate any change in chlorophyll specifically with ash arrival.~~

~~The change in chlorophyll-a observed in the SE Pacific contrasts with results in Reloncaví Fjord where phytoplankton abundances likely peaked much later than the first ash arrival after 28 April. The fertilized region of the Pacific (Fig. whilst also being proceeded by a larger chlorophyll-a peak on 21 April, there is a peak in chlorophyll-a at 25 April coinciding with elevated UV aerosol index). Phytoplankton growth in this region of the Atlantic is~~

Formatted: Font color: Black

Formatted: Normal, Border: Top: (No border), Bottom: (No border), Left: (No border), Right: (No border), Between : (No border), Tab stops: 3.25", Centered + 6.5", Right

764 expected to be limited by fixed nitrogen availability, as a result of strong stratification (Moore  
765 et al., 2013) and thus dFe release from ash particles alone would not be expected to result in  
766 short-term increases to primary production. In the second area of ash deposition, to the south  
767 (Sup. Fig. 3), a chlorophyll-a peak was evident 7 days after the UV aerosol peak. However,  
768 this was not well constrained due to poor satellite coverage in the period after the eruption.  
769 Considering the dynamic spatial and temporal variation in chlorophyll within this coastal  
770 area, it is challenging to associate any change in chlorophyll specifically with ash arrival.

771  
772 The change in chlorophyll-a observed in the SE Pacific contrasts with results in Reloncaví  
773 Fjord where phytoplankton abundances likely peaked much later than the first ash arrival-  
774 after 28 April. The fertilized region of the Pacific (Fig. 8) hosts upwelling of deep waters,  
775 supplying nutrients in ratios that are deficient in dFe (Bonnet et al., 2008; Torres and  
776 Ampuero, 2009). Fe-limitation of phytoplankton growth in this region is therefore  
777 anticipated, which could have been temporarily relieved following ash deposition and dFe  
778 release (Fig. 6). Conversely, ash deposition into the south western Atlantic indicated by the  
779 UV aerosol index did not lead to such a clear corresponding change in chlorophyll a  
780 concentrations (Fig. 8H), although with the available data it is not possible to rule out the  
781 possibility of fertilisation completely (e.g., whilst also being proceeded by a larger  
782 chlorophyll-a peak on August 21st, there is a peak in chlorophyll-a at August 25th coinciding  
783 with elevated UV aerosol index). Phytoplankton growth in this region of the Atlantic is  
784 expected to be limited by fixed nitrogen availability, as a result of strong stratification (Moore  
785 et al., 2013) and thus dFe release from ash particles would not be expected to result in short-  
786 term increases to primary production. The differential responses observed in the Pacific and

**Formatted:** Font color: Black

**Formatted:** Normal, Border: Top: (No border), Bottom: (No border), Left: (No border), Right: (No border), Between : (No border), Tab stops: 3.25", Centered + 6.5", Right

Atlantic are therefore consistent with the anticipated nutrient limitation regimes (Fe-limited and nitrogen-limited, respectively), and the supply of dFe but not fixed N ( $\text{NO}_3$  or  $\text{NH}_4$ ) from the Calbuco ash (Fig. 6 and Table 2).

## 5 Conclusions

The contrasting effects of volcanic ash on primary producers in Reloncaví Fjord, the SE Pacific and SW Atlantic Oceans support the hypothesis that the response of primary producers is dependent on both the ash loading and the resources limiting primary production in a region at a specific time of year. Leach experiments using ash from the 2015 Calbuco eruption demonstrated a small increase in the alkalinity of de-ionized water from fine, but not coarse ash, and no significant addition of fixed nitrogen (quantified as  $\text{NO}_3$  and  $\text{NH}_4$ ) into solution. In saline waters, release of dissolved trace metals including Mn, Cu, Co, Pb, Fe and specifically Fe(II) was evident.

Strong evidence of a broad-scale ‘bottom-up’ fertilization effect of ash on primary production was not found locally within Reloncaví Fjord, although it is possible that the timing and peak diatom abundance of the autumn phytoplankton bloom may have shifted in response to high ash loading in the weeks following the first eruption. High diatom abundances at some stations within the fjord several weeks after the eruption may have arisen from a ‘top-down’ effect of ash on filter feeders, although the mechanism can only be speculated herein. No clear positive effect of ash deposition on chlorophyll-a was evident in the SW Atlantic, consistent with expected patterns in nutrient deficiency which suggest the region to be nitrogen-limited. However, in offshore waters of the SE Pacific where Fe is anticipated to

**Formatted:** Font color: Black

**Formatted:** Normal, Border: Top: (No border), Bottom: (No border), Left: (No border), Right: (No border), Between : (No border), Tab stops: 3.25", Centered + 6.5", Right

limit phytoplankton growth, a chlorophyll-a increase was related with maximum ash deposition and we presume that this increase in chlorophyll-a was likely driven by Fe-fertilization.

## 6. Data availability

The complete 2015 time series from the Reloncaví Fjord mooring is available online ([https://figshare.com/articles/Puelo\\_Bouy/7754258](https://figshare.com/articles/Puelo_Bouy/7754258)). Source data for Figures 4-7 is included in the Supplement.

## 7. Acknowledgements

The authors thank the Dirección de Investigación & Desarrollo UCh for its partial support during this project. The data presented are part of the second chapter of the PhD Thesis of MVJ at Universidad Austral de Chile. Cristian Vargas (Universidad de Concepción) is thanked for making additional chlorophyll a data available, Manuel Díaz for providing Fig. 1 ~~and~~, [Lorena Rebolledo for running the particle size test](#), Miriam Beck for assistance with Fe(II) flow injection analysis [and 3 reviewers for constructive comments that improved the manuscript](#).

## 8. Funding

JLI and EA gratefully acknowledge funding from the European Commission (OCEAN-CERTAIN, FP7- ENV- 2013-6.1-1; no: 603773). JLI received funding by CONICYT-FONDECYT 1141065 and is partially funded by Center IDEAL (FONDAP 15150003). Partial funding came from CONICYT-FONDECYT 1140385 (RT). MVJ received financial

Formatted: Font color: Black

Formatted: Normal, Border: Top: (No border), Bottom: (No border), Left: (No border), Right: (No border), Between : (No border), Tab stops: 3.25", Centered + 6.5", Right

833 support from a CONICYT Scholarship (Beca Doctorado Nacional 2015 No 21150285). IR  
834 and MH received funding from the Deutsche Forschungsgemeinschaft as part of  
835 Sonderforschungsbereich (SFB) 754: 'Climate-Biogeochemistry Interactions in the Tropical  
836 Ocean'.

837

## 838 **9. Author contributions**

839 MVJ, MH, JLI and EA designed the study. MVJ, IR, MH, RT and BR conducted analytical  
840 and field work. TB conducted satellite data analysis. MV, MH and TB wrote the initial  
841 manuscript with all authors contributing to its revision.

842

## 843 **10. References**

844 Achterberg, E. ., Moore, C. M., Henson, S. A., Steigenberger, S., Stohl, A., Eckhardt, S.,  
845 Avendano, L. C., Cassidy, M., Hembury, D., Klar, J. K., Lucas, M. I., MacEy, A. I.,  
846 Marsay, C. M. and Ryan-Keogh, T. J.: Natural iron fertilization by the Eyjafjallajokull  
847 volcanic eruption, *Geophys. Res. Lett.*, 40(5), 921–926, doi:10.1002/grl.50221, 2013.  
848 Ahumada, R., Rudolph, A., Gonzalez, E., Fones, G., Saldias, G. and Ahumada Rudolph, R.:  
849 Dissolved trace metals in the water column of Reloncavi Fjord, Chile, *Lat. Am. J. Aquat.*  
850 *Res.*, 39, 567–574, doi:10.3856/vol39-issue3-fulltext-16, 2011.  
851 Ayrís, P. and Delmelle, P.: Volcanic and atmospheric controls on ash iron solubility: A  
852 review, *Phys. Chem. Earth*, doi:10.1016/j.pce.2011.04.013, 2012.  
853 Baker, A. R. and Croot, P. L.: Atmospheric and marine controls on aerosol iron solubility  
854 in seawater, *Mar. Chem.*, 120(1–4), 4–13, doi:10.1016/j.marchem.2008.09.003, 2010.  
855 Balseiro, E., Souza, M. S., Olabuenaga, I. S., Wolinski, L., Navarro, M. B.,

**Formatted:** Font color: Black

**Formatted:** Normal, Border: Top: (No border), Bottom: (No border), Left: (No border), Right: (No border), Between : (No border), Tab stops: 3.25", Centered + 6.5", Right



856 Laspoumaderes, C. and Modenutti, B.: Effect of the Puyehue-Cordon Caulle volcanic  
 857 complex eruption on crustacean zooplankton of Andean Lakes, *Ecol. Austral*, 24, 75–82,  
 858 2014.

859 Bonnet, S., Guieu, C., Bruyant, F., Prášil, O., Van Wambeke, F., Raimbault, P., Moutin, T.,  
 860 Grob, C., Gorbunov, M. Y., Zehr, J. P., Masquelier, S. M., Garczarek, L. and Claustre, H.:  
 861 Nutrient limitation of primary productivity in the Southeast Pacific (BIOCOPE cruise),  
 862 *Biogeosciences*, 5(1), 215–225, doi:10.5194/bg-5-215-2008, 2008.

863 Boyle, E. A., Edmond, J. M. and Sholkovitz, E. R.: Mechanism of iron removal in  
 864 estuaries, *Geochim. Cosmochim. Acta*, 41(9), 1313–1324, doi:10.1016/0016-  
 865 7037(77)90075-8, 1977.

866 Browning, T. J., Bouman, H. A., Henderson, G. M., Mather, T. A., Pyle, D. M., Schlosser,  
 867 C., Woodward, E. M. S. and Moore, C. M.: Strong responses of Southern Ocean  
 868 phytoplankton communities to volcanic ash, *Geophys. Res. Lett.*, 41(8), 2851–2857,  
 869 doi:10.1002/2014GL059364, 2014.

870 Browning, T. J., Stone, K., Bouman, H., Mather, T. A., Pyle, D. M., Moore, M. and  
 871 Martinez-Vicente, V.: Volcanic ash supply to the surface ocean – remote sensing of  
 872 biological responses and their wider biogeochemical significance, *Front. Mar. Sci.*, 2,  
 873 doi:10.3389/fmars.2015.00014, 2015.

874 Brzezinski, M. A.: The Si:C:N ratio of marine diatoms: interspecific variability and the  
 875 effect of some environmental variables, *J. Phycol.*, 21(3), 347–357, doi:10.1111/j.0022-  
 876 3646.1985.00347.x, 1985.

877 Buck, C. S., Landing, W. M. and Resing, J.: Pacific Ocean aerosols: Deposition and  
 878 solubility of iron, aluminum, and other trace elements, *Mar. Chem.*, 157, 117–130,

**Formatted:** Font color: Black

**Formatted:** Normal, Border: Top: (No border), Bottom: (No border), Left: (No border), Right: (No border), Between : (No border), Tab stops: 3.25", Centered + 6.5", Right

879 doi:10.1016/j.marchem.2013.09.005, 2013.

880 Cáceres, M., Valle-Levinson, A., Sepúlveda, H. H. and Holderied, K.: Transverse  
881 variability of flow and density in a Chilean fjord, in *Continental Shelf Research.*, 2002.

882 Castillo, M. I., Cifuentes, U., Pizarro, O., Djurfeldt, L. and Cáceres, M.: Seasonal  
883 hydrography and surface outflow in a fjord with a deep sill: The Reloncaví fjord, Chile,  
884 *Ocean Sci.*, 12, 533–544, doi:10.5194/os-12-533-2016, 2016.

885 DeGrandpre, M. D., Hammar, T. R., Smith, S. P. and Sayles, F. L.: In situ measurements of  
886 seawater pCO<sub>2</sub>, *Limnol. Oceanogr.*, 40(5), 969–975, doi:10.4319/lo.1995.40.5.0969, 1995.

887 DeGrandpre, M. D., Baehr, M. M. and Hammar, T. R.: Calibration-free optical chemical  
888 sensors, *Anal. Chem.*, 71(6), 1152–1159, doi:10.1021/ac9805955, 1999.

889 Delmelle, P., Lambert, M., Dufrêne, Y., Gerin, P. and Óskarsson, N.: Gas/aerosol-ash  
890 interaction in volcanic plumes: New insights from surface analyses of fine ash particles,  
891 *Earth Planet. Sci. Lett.*, 259, 159–170, doi:10.1016/j.epsl.2007.04.052, 2007.

892 Duggen, S., Croot, P., Schacht, U. and Hoffmann, L.: Subduction zone volcanic ash can  
893 fertilize the surface ocean and stimulate phytoplankton growth: Evidence from  
894 biogeochemical experiments and satellite data, *Geophys. Res. Lett.*,  
895 doi:10.1029/2006GL027522, 2007.

896 Duggen, S., Olgun, N., Croot, P., Hoffmann, L., Dietze, H., Delmelle, P. and Teschner, C.:  
897 The role of airborne volcanic ash for the surface ocean biogeochemical iron-cycle: a  
898 review, *Biogeosciences*, 7(3), 827–844, doi:10.5194/bg-7-827-2010, 2010.

899 Van Eaton, A. R., Amigo, Á., Bertin, D., Mastin, L. G., Giacosa, R. E., González, J.,  
900 Valderrama, O., Fontijn, K. and Behnke, S. A.: Volcanic lightning and plume behavior  
901 reveal evolving hazards during the April 2015 eruption of Calbuco volcano, Chile,

**Formatted:** Font color: Black

**Formatted:** Normal, Border: Top: (No border), Bottom: (No border), Left: (No border), Right: (No border), Between : (No border), Tab stops: 3.25", Centered + 6.5", Right

902 Geophys. Res. Lett., 43(7), 3563–3571, doi:10.1002/2016GL068076, 2016.

903 Ermolin, M. S., Fedotov, P. S., Malik, N. A. and Karandashev, V. K.: Nanoparticles of  
 904 volcanic ash as a carrier for toxic elements on the global scale, Chemosphere, 200, 16–22,  
 905 doi:10.1016/j.chemosphere.2018.02.089, 2018.

906 Frogner, P., Gislason, S. R. and Oskarsson, N.: Fertilizing potential of volcanic ash in  
 907 ocean surface water, Geology, 29(6), 487–490, doi:10.1130/0091-  
 908 7613(2001)029<0487:fpovai>2.0.co;2, 2001.

909 Gledhill, M. and Buck, K. N.: The organic complexation of iron in the marine environment:  
 910 a review, Front. Microbiol., 3, 69, doi:10.3389/fmicb.2012.00069, 2012.

911 González, H. E., Calderón, M. J., Castro, L., Clement, A., Cuevas, L. A., Daneri, G., Iriarte,  
 912 J. L., Lizárraga, L., Martínez, R., Menschel, E., Silva, N., Carrasco, C., Valenzuela, C.,  
 913 Vargas, C. A. and Molinet, C.: Primary production and plankton dynamics in the Reloncaví  
 914 Fjord and the Interior Sea of Chiloé, Northern Patagonia, Chile, Mar. Ecol. Prog. Ser., 402,  
 915 13–30, 2010.

916 Hamme, R. C., Webley, P. W., Crawford, W. R., Whitney, F. A., Degrandpre, M. D.,  
 917 Emerson, S. R., Eriksen, C. C., Giesbrecht, K. E., Gower, J. F. R., Kavanaugh, M. T., Pea,  
 918 M. A., Sabine, C. L., Batten, S. D., Coogan, L. A., Grundle, D. S. and Lockwood, D.:  
 919 Volcanic ash fuels anomalous plankton bloom in subarctic northeast Pacific, Geophys. Res.  
 920 Lett., 37(19), L19604, doi:10.1029/2010GL044629, 2010.

921 Haraldsson, C., Anderson, L. G., Hassellöv, M., Hulth, S. and Olsson, K.: Rapid, high-  
 922 precision potentiometric titration of alkalinity in ocean and sediment pore waters, Deep Sea  
 923 Res. Part I Oceanogr. Res. Pap., 44(12), 2031–2044, doi:10.1016/S0967-0637(97)00088-5,  
 924 1997.

**Formatted:** Font color: Black

**Formatted:** Normal, Border: Top: (No border), Bottom: (No border), Left: (No border), Right: (No border), Between : (No border), Tab stops: 3.25", Centered + 6.5", Right

925 Hoffmann, L. J., Breitbarth, E., Ardelan, M. V., Duggen, S., Olgun, N., Hassellöv, M. and  
 926 Wängberg, S.-Å.: Influence of trace metal release from volcanic ash on growth of  
 927 *Thalassiosira pseudonana* and *Emiliania huxleyi*, *Mar. Chem.*, 132–133, 28–33,  
 928 doi:10.1016/j.marchem.2012.02.003, 2012.

929 Hopwood, M. J., Santana-González, C., Gallego-Urrea, J., Sanchez, N., Achterberg, E. P.,  
 930 Ardelan, M. V., Gledhill, M., González-Dávila, M., Hoffmann, L., Leiknes, Ø., Magdalena  
 931 Santana-Casiano, J., Tsagaraki, T. M. and Turner, D.: Fe(II) stability in coastal seawater  
 932 during experiments in Patagonia, Svalbard, and Gran Canaria, *Biogeosciences*,  
 933 doi:10.5194/bg-17-1327-2020, 2020.

934 Horwell, C. J., Fenoglio, I., Vala Ragnarsdottir, K., Sparks, R. S. J. and Fubini, B.: Surface  
 935 reactivity of volcanic ash from the eruption of Soufrière Hills volcano, Montserrat, West  
 936 Indies with implications for health hazards, *Environ. Res.*, 93(2), 202–215,  
 937 doi:10.1016/S0013-9351(03)00044-6, 2003.

938 Hoshyaripour, G. A., Hort, M. and Langmann, B.: Ash iron mobilization through  
 939 physicochemical processing in volcanic eruption plumes: A numerical modeling approach,  
 940 *Atmos. Chem. Phys.*, 15, 9361–9379, doi:10.5194/acp-15-9361-2015, 2015.

941 Hu, C., Lee, Z. and Franz, B.: Chlorophyll algorithms for oligotrophic oceans: A novel  
 942 approach based on three-band reflectance difference, *J. Geophys. Res. Ocean.*, 117(C1),  
 943 doi:10.1029/2011JC007395, 2012.

944 Iriarte, J. L., González, H. E., Liu, K. K., Rivas, C. and Valenzuela, C.: Spatial and  
 945 temporal variability of chlorophyll and primary productivity in surface waters of southern  
 946 Chile (41.5–43° S), *Estuar. Coast. Shelf Sci.*, 74(3), 471–480,  
 947 doi:10.1016/j.ecss.2007.05.015, 2007.

**Formatted:** Font color: Black

**Formatted:** Normal, Border: Top: (No border), Bottom: (No border), Left: (No border), Right: (No border), Between : (No border), Tab stops: 3.25", Centered + 6.5", Right

948 Jones, M. R., Nightingale, P. D., Turner, S. M. and Liss, P. S.: Adaptation of a load-inject  
 949 valve for a flow injection chemiluminescence system enabling dual-reagent injection  
 950 enhances understanding of environmental Fenton chemistry, *Anal. Chim. Acta*, 796, 55–60,  
 951 doi:10.1016/j.aca.2013.08.003, 2013.

952 Jones, M. T. and Gislason, S. R.: Rapid releases of metal salts and nutrients following the  
 953 deposition of volcanic ash into aqueous environments, *Geochim. Cosmochim. Acta*, 72(15),  
 954 3661–3680, doi:10.1016/j.gca.2008.05.030, 2008.

955 Labbé-Ibáñez, P., Iriarte, J. L. and Pantoja, S.: Respuesta del microfitoplancton a la adición  
 956 de nitrato y ácido silícico en fiordos de la Patagonia chilena, *Lat. Am. J. Aquat. Res.*, 43(1),  
 957 80–93, doi:10.3856/vol43-issue1-fulltext-8, 2015.

958 Langmann, B., Zakšek, K., Hort, M. and Duggen, S.: Volcanic ash as fertiliser for the  
 959 surface ocean, *Atmos. Chem. Phys.*, 10, 3891–3899, doi:10.5194/acp-10-3891-2010, 2010.

960 León-Muñoz, J., Marcé, R. and Iriarte, J. L.: Influence of hydrological regime of an Andean  
 961 river on salinity, temperature and oxygen in a Patagonia fjord, Chile, *New Zeal. J. Mar.*  
 962 *Freshw. Res.*, 47(4), 515–528, doi:10.1080/00288330.2013.802700, 2013.

963 León-Muñoz, J., Urbina, M. A., Garreaud, R. and Iriarte, J. L.: Hydroclimatic conditions  
 964 trigger record harmful algal bloom in western Patagonia (summer 2016), *Sci. Rep.*, 8(1),  
 965 1330, doi:10.1038/s41598-018-19461-4, 2018.

966 Lin, I. I., Hu, C., Li, Y. H., Ho, T. Y., Fischer, T. P., Wong, G. T. F., Wu, J., Huang, C. W.,  
 967 Chu, D. A., Ko, D. S. and Chen, J. P.: Fertilization potential of volcanic dust in the low-  
 968 nutrient low-chlorophyll western North Pacific subtropical gyre: Satellite evidence and  
 969 laboratory study, *Global Biogeochem. Cycles*, 25, GB1006, doi:10.1029/2009GB003758,  
 970 2011.

**Formatted:** Font color: Black

**Formatted:** Normal, Border: Top: (No border), Bottom: (No border), Left: (No border), Right: (No border), Between : (No border), Tab stops: 3.25", Centered + 6.5", Right

971 López-Escobar, L., Parada, M. A., Hickey-Vargas, R., Frey, F. A., Kempton, P. D. and  
 972 Moreno, H.: Calbuco Volcano and minor eruptive centers distributed along the Liquiñe-  
 973 Ofqui Fault Zone, Chile (41°–42° S): contrasting origin of andesitic and basaltic magma in  
 974 the Southern Volcanic Zone of the Andes, *Contrib. to Mineral. Petrol.*, 119(4), 345–361,  
 975 doi:10.1007/BF00286934, 1995.  
 976 Martin, J. H., Fitzwater, S. E. and Gordon, R. M.: Iron deficiency limits phytoplankton  
 977 growth in Antarctic waters, *Global Biogeochem. Cycles*, 4(1), 5–12, 1990.  
 978 Maters, E. C., Delmelle, P. and Gunnlaugsson, H. P.: Controls on iron mobilisation from  
 979 volcanic ash at low pH: Insights from dissolution experiments and Mössbauer  
 980 spectroscopy, *Chem. Geol.*, 449, 73–81, doi:10.1016/j.chemgeo.2016.11.036, 2017.  
 981 Mélançon, J., Levasseur, M., Lizotte, M., Delmelle, P., Cullen, J., Hamme, R. C., Peña, A.,  
 982 Simpson, K. G., Scarratt, M., Tremblay, J. É., Zhou, J., Johnson, K., Sutherland, N.,  
 983 Arychuk, M., Nemcek, N. and Robert, M.: Early response of the northeast subarctic Pacific  
 984 plankton assemblage to volcanic ash fertilization, *Limnol. Oceanogr.*, 59,  
 985 doi:10.4319/lo.2014.59.1.0055, 2014.  
 986 Mendez, J., Guieu, C. and Adkins, J.: Atmospheric input of manganese and iron to the  
 987 ocean: Seawater dissolution experiments with Saharan and North American dusts, *Mar.*  
 988 *Chem.*, 120(1), 34–43, doi:10.1016/j.marchem.2008.08.006, 2010.  
 989 Millero, F. J., Sotolongo, S. and Izaguirre, M.: The oxidation-kinetics of Fe(II) in seawater,  
 990 *Geochim. Cosmochim. Acta*, 51(4), 793–801, doi:10.1016/0016-7037(87)90093-7, 1987.  
 991 Molinet, C., Díaz, M., Marín, S. L., Astorga, M. P., Ojeda, M., Cares, L. and Asencio, E.:  
 992 Relation of mussel spatfall on natural and artificial substrates: Analysis of ecological  
 993 implications ensuring long-term success and sustainability for mussel farming,

**Formatted:** Font color: Black

**Formatted:** Normal, Border: Top: (No border), Bottom: (No border), Left: (No border), Right: (No border), Between : (No border), Tab stops: 3.25", Centered + 6.5", Right

994 Aquaculture, 467, 211–218, doi:10.1016/j.aquaculture.2016.09.019, 2017.

995 Moore, C. M., Mills, M. M., Arrigo, K. R., Berman-Frank, I., Bopp, L., Boyd, P. W.,

996 Galbraith, E. D., Geider, R. J., Guieu, C., Jaccard, S. L., Jickells, T. D., La Roche, J.,

997 Lenton, T. M., Mahowald, N. M., Marañón, E., Marinov, I., Moore, J. K., Nakatsuka, T.,

998 Oschlies, A., Saito, M. A., Thingstad, T. F., Tsuda, A. and Ulloa, O.: Processes and

999 patterns of oceanic nutrient limitation, Nat. Geosci., doi:10.1038/ngeo1765, 2013.

1000 Morton, P. L., Landing, W. M., Hsu, S. C., Milne, A., Aguilar-Islas, A. M., Baker, A. R.,

1001 Bowie, A. R., Buck, C. S., Gao, Y., Gichuki, S., Hastings, M. G., Hatta, M., Johansen, A.

1002 M., Losno, R., Mead, C., Patey, M. D., Swarr, G., Vandermark, A. and Zamora, L. M.:  
 1003 Methods for the sampling and analysis of marine aerosols: Results from the 2008  
 1004 GEOTRACES aerosol intercalibration experiment, Limnol. Oceanogr. Methods, 11,  
 1005 doi:10.4319/lom.2013.11.62, 2013.

1006 Mosley, L. M., Husheer, S. L. G. and Hunter, K. A.: Spectrophotometric pH measurement  
 1007 in estuaries using thymol blue and m-cresol purple, Mar. Chem., 91, 175–186,  
 1008 doi:10.1016/j.marchem.2004.06.008, 2004.

1009 Newcomb, T. W. and Flagg, T. A.: Some effects of Mt. St. Helens volcanic ash on juvenile  
 1010 salmon smolts., Mar. Fish. Rev., 45(2), 8–12, 1983.

1011 Olgun, N., Duggen, S., Croot, P. L., Delmelle, P., Dietze, H., Schacht, U., Óskarsson, N.,  
 1012 Siebe, C., Auer, A. and Garbe-Schönberg, D.: Surface ocean iron fertilization: The role of  
 1013 airborne volcanic ash from subduction zone and hot spot volcanoes and related iron fluxes  
 1014 into the Pacific Ocean, Global Biogeochem. Cycles, 25(4), doi:10.1029/2009GB003761,  
 1015 2011.

1016 Olsson, J., Stipp, S. L. S., Dalby, K. N. and Gislason, S. R.: Rapid release of metal salts and

**Formatted:** Font color: Black

**Formatted:** Normal, Border: Top: (No border), Bottom: (No border), Left: (No border), Right: (No border), Between : (No border), Tab stops: 3.25", Centered + 6.5", Right

1017 nutrients from the 2011 Grímsvötn, Iceland volcanic ash, *Geochim. Cosmochim. Acta*,  
 1018 doi:10.1016/j.gca.2013.09.009, 2013.

1019 Óskarsson, N.: The interaction between volcanic gases and tephra: Fluorine adhering to  
 1020 tephra of the 1970 Hekla eruption, *J. Volcanol. Geotherm. Res.*, doi:10.1016/0377-  
 1021 0273(80)90107-9, 1980.

1022 Rapp, I., Schlosser, C., Rusiecka, D., Gledhill, M. and Achterberg, E. P.: Automated  
 1023 preconcentration of Fe, Zn, Cu, Ni, Cd, Pb, Co, and Mn in seawater with analysis using  
 1024 high-resolution sector field inductively-coupled plasma mass spectrometry, *Anal. Chim.*  
 1025 *Acta*, 976, 1–13, doi:10.1016/j.aca.2017.05.008, 2017.

1026 Reckziegel, F., Bustos, E., Mingari, L., Báez, W., Villarosa, G., Folch, A., Collini, E.,  
 1027 Viramonte, J., Romero, J. and Osores, S.: Forecasting volcanic ash dispersal and coeval  
 1028 resuspension during the April-May 2015 Calbuco eruption, *J. Volcanol. Geotherm. Res.*,  
 1029 doi:10.1016/j.jvolgeores.2016.04.033, 2016.

1030 Rogan, N., Achterberg, E. P., Le Moigne, F. A. C., Marsay, C. M., Tagliabue, A. and  
 1031 Williams, R. G.: Volcanic ash as an oceanic iron source and sink, *Geophys. Res. Lett.*,  
 1032 43(6), 2732–2740, doi:10.1002/2016GL067905, 2016.

1033 Romero, J. E., Morgavi, D., Arzilli, F., Daga, R., Caselli, A., Reckziegel, F., Viramonte, J.,  
 1034 Díaz-Alvarado, J., Polacci, M., Burton, M. and Perugini, D.: Eruption dynamics of the 22–  
 1035 23 April 2015 Calbuco Volcano (Southern Chile): Analyses of tephra fall deposits, *J.*  
 1036 *Volcanol. Geotherm. Res.*, 317, 15–29, doi:10.1016/j.jvolgeores.2016.02.027, 2016.

1037 Rubin, C. H., Noji, E. K., Seligman, P. J., Holtz, J. L., Grande, J. and Vittani, F.:  
 1038 Evaluating a fluorosis hazard after a volcanic eruption, *Arch. Environ. Health*,  
 1039 doi:10.1080/00039896.1994.9954992, 1994.

**Formatted:** Font color: Black

**Formatted:** Normal, Border: Top: (No border), Bottom: (No border), Left: (No border), Right: (No border), Between : (No border), Tab stops: 3.25", Centered + 6.5", Right



1040 Sanchez, N., Bizsel, N., Iriarte, J. L., Olsen, L. M. and Ardelan, M. V.: Iron cycling in a  
1041 mesocosm experiment in a north Patagonian fjord: Potential effect of ammonium addition  
1042 by salmon aquaculture, *Estuar. Coast. Shelf Sci.*, 220, 209–219,  
1043 doi:10.1016/j.ecss.2019.02.044, 2019.

1044 Santana-Casiano, J. M., Gonzalez-Davila, M. and Millero, F. J.: Oxidation of nanomolar  
1045 levels of Fe(II) with oxygen in natural waters, *Environ. Sci. Technol.*, 39(7), 2073–2079,  
1046 doi:10.1021/es049748y, 2005.

1047 Sarmiento, J. L.: Atmospheric CO<sub>2</sub> stalled, *Nature*, doi:10.1038/365697a0, 1993.

1048 Sarthou, G., Bucciarelli, E., Chever, F., Hansard, S. P., Gonzalez-Davila, M., Santana-  
1049 Casiano, J. M., Planchon, F. and Speich, S.: Labile Fe(II) concentrations in the Atlantic  
1050 sector of the Southern Ocean along a transect from the subtropical domain to the Weddell  
1051 Sea Gyre, *Biogeosciences*, 8(9), 2461–2479, doi:10.5194/bg-8-2461-2011, 2011.

1052 Seidel, M. P., DeGrandpre, M. D. and Dickson, A. G.: A sensor for in situ indicator-based  
1053 measurements of seawater pH, *Mar. Chem.*, 109(1), 18–28,  
1054 doi:10.1016/j.marchem.2007.11.013, 2008.

1055 Simonella, L. E., Palomeque, M. E., Croot, P. L., Stein, A., Kupczewski, M., Rosales, A.,  
1056 Montes, M. L., Colombo, F., García, M. G., Villarosa, G. and Gaiero, D. M.: Soluble iron  
1057 inputs to the Southern Ocean through recent andesitic to rhyolitic volcanic ash eruptions  
1058 from the Patagonian Andes, *Global Biogeochem. Cycles*, 29(8), 1125–1144,  
1059 doi:10.1002/2015GB005177, 2015.

1060 Siringan, F. P., Racasa, E. D. R., David, C. P. C. and Saban, R. C.: Increase in Dissolved  
1061 Silica of Rivers Due to a Volcanic Eruption in an Estuarine Bay (Sorsogon Bay,  
1062 Philippines), *Estuaries and Coasts*, 41, 2277–2288, doi:10.1007/s12237-018-0428-1, 2018.

**Formatted:** Font color: Black

**Formatted:** Normal, Border: Top: (No border), Bottom: (No border), Left: (No border), Right: (No border), Between : (No border), Tab stops: 3.25", Centered + 6.5", Right

1063 Stewart, C., Johnston, D. M., Leonard, G. S., Horwell, C. J., Thordarson, T. and Cronin, S.  
 1064 J.: Contamination of water supplies by volcanic ashfall: A literature review and simple  
 1065 impact modelling, *J. Volcanol. Geotherm. Res.*, 158(3), 296–306,  
 1066 doi:10.1016/j.jvolgeores.2006.07.002, 2006.

1067 Sunda, W. G., Buffle, J. and Van Leeuwen, H. P.: Bioavailability and Bioaccumulation of  
 1068 Iron in the Sea, in *The Biogeochemistry of Iron in Seawater*, vol. 7, edited by D. R. Turner  
 1069 and K. A. Hunter, pp. 41–84, John Wiley & Sons, Ltd, Chichester., 2001.

1070 Torres, O., Tanskanen, A., Veihelmann, B., Ahn, C., Braak, R., Bhartia, P. K., Veefkind, P.  
 1071 and Levelt, P.: Aerosols and surface UV products from Ozone Monitoring Instrument  
 1072 observations: An overview, *J. Geophys. Res. Atmos.*, doi:10.1029/2007JD008809, 2007.

1073 Torres, R. and Ampuero, P.: Strong CO<sub>2</sub> outgassing from high nutrient low chlorophyll  
 1074 coastal waters off central Chile (30°S): The role of dissolved iron, *Estuar. Coast. Shelf Sci.*,  
 1075 83(2), 126–132, doi:10.1016/j.ecss.2009.02.030, 2009.

1076 Torres, R., Silva, N., Reid, B. and Frangopulos, M.: Silicic acid enrichment of subantarctic  
 1077 surface water from continental inputs along the Patagonian archipelago interior sea (41-  
 1078 56°S), *Prog. Oceanogr.*, 129, 50–61, doi:10.1016/j.pocean.2014.09.008, 2014.

1079 Utermöhl, H.: Zur Vervollkommnung der quantitativen Phytoplankton-Methodik, *SIL*  
 1080 *Commun.* 1953-1996, doi:10.1080/05384680.1958.11904091, 1958.

1081 Vergara-Jara, M. J., DeGrandpre, M. D., Torres, R., Beatty, C. M., Cuevas, L. A., Alarcón,  
 1082 E. and Iriarte, J. L.: Seasonal Changes in Carbonate Saturation State and Air-Sea CO<sub>2</sub>  
 1083 Fluxes During an Annual Cycle in a Stratified-Temperate Fjord (Reloncaví Fjord, Chilean  
 1084 Patagonia), *J. Geophys. Res. Biogeosciences*, 124(9), 2851–2865,  
 1085 doi:10.1029/2019JG005028, 2019.

**Formatted:** Font color: Black

**Formatted:** Normal, Border: Top: (No border), Bottom: (No border), Left: (No border), Right: (No border), Between : (No border), Tab stops: 3.25", Centered + 6.5", Right

1086 Watson, A. J.: Volcanic iron, CO<sub>2</sub>, ocean productivity and climate, *Nature*,  
1087 doi:10.1038/385587b0, 1997.

1088 Weinbauer, M. G., Guinot, B., Migon, C., Malfatti, F. and Mari, X.: Skyfall - neglected  
1089 roles of volcano ash and black carbon rich aerosols for microbial plankton in the ocean, *J.*  
1090 *Plankton Res.*, 39(2), 187–198, doi:10.1093/plankt/fbw100, 2017.

1091 Welschmeyer, N. A.: Fluorometric analysis of chlorophyll a in the presence of chlorophyll  
1092 b and pheopigments, *Limnol. Oceanogr.*, doi:10.4319/lo.1994.39.8.1985, 1994.

1093 Witham, C. S., Oppenheimer, C. and Horwell, C. J.: Volcanic ash-leachates: a review and  
1094 recommendations for sampling methods, *J. Volcanol. Geotherm. Res.*, 141(3), 299–326,  
1095 doi:10.1016/j.jvolgeores.2004.11.010, 2005.

1096 Wolinski, L., Laspoumaderes, C., Bastidas Navarro, M., Modenutti, B. and Balseiro, E.:  
1097 The susceptibility of cladocerans in North Andean Patagonian lakes to volcanic ashes,  
1098 *Freshw. Biol.*, 58, 1878–1888, doi:10.1111/fwb.12176, 2013.

1099 Yevenes, M. A., Lagos, N. A., Farías, L. and Vargas, C. A.: Greenhouse gases, nutrients  
1100 and the carbonate system in the Reloncaví Fjord (Northern Chilean Patagonia):  
1101 Implications on aquaculture of the mussel, *Mytilus chilensis*, during an episodic volcanic  
1102 eruption, *Sci. Total Environ.*, doi:10.1016/j.scitotenv.2019.03.037, 2019.

1103

**Formatted:** Font color: Black

**Formatted:** Normal, Border: Top: (No border), Bottom: (No border), Left: (No border), Right: (No border), Between : (No border), Tab stops: 3.25", Centered + 6.5", Right